Ocean Modelling
June 2019, Volume 138, Pages 23-35
https://doi.org/10.1016/j.ocemod.2019.04.004
https://archimer.ifremer.fr/doc/00494/60525/

Potential Vorticity diagnostics based on balances between volume integral and boundary conditions

Morel Yves [1, *], Gula Jonathan [2], Ponte Aurelien [3]

[1] LEGOS, Université de Toulouse, CNES, CNRS, IRD, UPS, Toulouse 31400, France
[2] LOPS, Université de Brest, CNRS, Ifremer, IRD, IUEM, Brest 29280, France

* Corresponding author : Yves Morel, email address : yves.morel@shom.fr

Abstract :

Taking advantage of alternative expressions for potential vorticity (PV) in divergence forms, we derive balances between volume integral of PV and boundary conditions, that are then applied to practical computations of PV:

• we propose a new method for diagnosing the Ertel potential vorticity from model output, that preserves the balances;

• we show how the expression of PV can be derived in general coordinate systems. This is here emphasised with isopycnic coordinates by generalising the PV expression to the general Navier-Stokes equations;

• we propose a generalised derivation for the Haynes-McIntyre impermeability theorem, which highlights the role of the bottom boundary condition choice (e.g. no-slip vs free-slip) and mixing near the bottom boundary for the volume integral of PV.

The implications of balances between volume integral of PV and boundary conditions are then analysed for specific processes at various scales:

• at large scale, we show how an integral involving surface observations (derived from satellite observations) is linked to the integral of PV within a layer (between two isopycnals). This surface integral can be calculated for models and observations and can be used for validation;

• at mesoscale or sub-mesoscale, we analyse the relationship between net PV anomalies and net surface density anomalies for idealised vortices and 2D fronts. This can help determining vortex or jet structures for idealised studies or empirical methodologies;

• we also confirm and integrate previous results on the modification of PV within a bottom boundary layer into a single diagnostic taking into account the effect of density and velocity modifications by diabatic processes along the topography and diapycnal mixing within the boundary layer.

Highlights

► Ertel potential vorticity (PV) expressions in divergence form improve PV diagnostics in models. ► Balances are derived between volume integral of PV and boundary conditions. ► Practical numerical computations of PV, preserving balances, are proposed. ► The implications of balances are examined for selected processes.

Keywords : Potential vorticity, boundary conditions, general circulation, vortex, fronts, boundary layers.

1. Introduction

It is well known that Ertel's Potential Vorticity (PV, see Ertel, 1942) is an important quantity when studying the circulation at all scales in geophysical fluids: the conservation property of PV -in adiabatic evolution- and the inversion principle (the geostrophic velocity field can be inferred from the PV field and boundary conditions) are key principles to interpret the ocean dynamics (see Hoskins et al., 1985; McWilliams, 2006, and section 2 for more details). Conservation and inversion of PV are the basis of the

quasigeostrophic (QG) model (Pedlosky, 1987) that has been successfully used in pioneering studies aiming at understanding and modelling the ocean circulation from basin gyres (Rhines and Young, 1982a,b; Luyten et al., 1983; Holland et al., 1984; Rhines, 1986; Talley, 1988; Marshall and Nurser, 1992) to current instabilities (Charney and Stern, 1962), geophysical turbulence (McWilliams, 1984) and mesoscale dynamics (McWilliams and Flierl, 1979; Sutyrin and Flierl, 1994).

In the QG framework, PV is related to the streamfunction by a linear elliptic differential operator (Pedlosky, 1987; Cushman-Roisin and Beckers, 2011), which has several important consequences. First, boundary conditions impose important dynamical constraints too. In a QG framework Bretherton (1966) has shown that surface or bottom outcropping of isopycnic surfaces is dynamically similar to a shallow layer of high PV anomaly (in practice a Dirac delta sheet), whose strength can be related to the density anomaly. This has led to the generalised surface quasigeostrophic (SQG) model (Held et al., 1995; Lapeyre, 2017). Lateral boundaries can be important too for the inversion of PV. In the QG or SQG framework, it has been shown that the velocity field away from a region of PV anomalies decreases slowly -as the inverse of the distance from the region- unless PV and surface density satisfy an integral constraint (Morel and McWilliams, 1997; Assassi et al., 2016). In models, practical inversion of PV, with given surface and bottom density fields, is often done considering biperiodic domains (Lapeyre et al., 2006; Wang et al., 2013), which can lead to discrepancies if the latter constraint is not satisfied.

Second, since the relationship between PV and the circulation is linear at first order (QG and SQG), the balance between smoothed/averaged fields is preserved, provided averaging is done using a linear convolution.

Moreover, PV concept is also useful for forced dissipative dynamics. For instance, diapycnal mixing does not change the volume integral of PV within a layer bounded by isopycnic surfaces, which shows that PV can only be diluted or concentrated when the layer respectively gains or looses mass (Haynes and McIntyre, 1987, 1990). The influence of viscous surface or bottom stress on the PV evolution has also been analysed theoretically (Thomas, 2005; Taylor and Ferrari, 2010; Benthuysen and Thomas, 2012, 2013). Thus, the consequences of diabatic effects on the ocean dynamics can again be analysed and interpreted in terms of PV modification from basin scales (see for instance Hallberg and Rhines, 1996, 2000; Czaja and Hausmann, 2009) to meso and submesoscales (see for instance Morel and McWilliams, 2001; Morel et al., 2006; Morel and Thomas, 2009; Rossi et al., 2010; Meunier et al., 2010; Thomas et al., 2013; Molemaker et al., 2015; Gula et al., 2015, 2016, 2019; Vic et al., 2015; Giordani et al., 2017).

To conclude, the ocean circulation and PV are linked and calculating PV at all scales under adiabatic or diabatic conditions is thus of considerable interest for geophysical fluid dynamics. In QG or SQG models, it is possible to ensure consistent balances between circulation, PV and surface, bottom and lateral boundary conditions, from local to averaged fields. In more complex models, PV calculation involves many velocity and density derivatives, in particular in non-isopycnic models, and keeping the link between averaged PV and averaged circulation implies to find a consistent calculation of PV. If several studies have used diagnostics involving PV, they remain rare and none have discussed the PV calculations in details, in particular to evaluate if the relationships between PV and boundary conditions are maintained and if averaging can be done consistently.

The Bretherton principle (Bretherton, 1966) has been recently revisited

and extended by Schneider et al. (2003) who generalised the concept of PV to take into account the dynamical effect of outcropping for the general Navier Stokes equations. To do so, they used the alternative divergence form for the expression of PV (Vallis, 2006). In this paper, we show how this divergence form of PV naturally leads to general constraints on volume balances of PV and boundary conditions (section 3). These follow from the definition of PV and are independent of the dynamics (adiabatic or diabatic) of the flow. In section 4 we show that the divergence form also makes PV computations easier and consistent, in the sense that balances are automatically preserved when integrating PV (a consequence of the divergence form). We then propose several frameworks, involving dynamics at different scales, to discuss the generalised constraints between PV and surface, bottom or lateral boundary conditions (section 5). We summarise and discuss our results in the concluding section. Section 2 summarises basic definitions and properties of PV which are not new and can be skipped by readers familiar with PV.

2. Reminders on potential vorticity

2.1. Definition of Ertel potential vorticity

Ertel (1942) defined Potential Vorticity as:

$$\begin{aligned} PV_{Ertel} &\equiv -(\vec{\nabla} \times \vec{U} + \vec{f}).\frac{\vec{\nabla}\rho}{\rho} \\ &= -(\vec{\nabla} \times \vec{U}_a).\frac{\vec{\nabla}\rho}{\rho} \end{aligned} \tag{1}$$

where $\vec{U}$ is the fluid velocity field in the reference frame of the rotating Earth, ρ is the potential density (in the ocean and entropy in the atmosphere),

$\vec{U}_a = \vec{U} + \vec{\Omega} \times \vec{r}$ is the absolute velocity, where $\vec{\Omega} = (0, \Omega_y, \Omega_z)$ is the rotation vector of the Earth, $\vec{r}$ is the position relative to the Earth center and $\vec{f} = (0, f_y, f_z) = \vec{\nabla} \times (\vec{\Omega} \times \vec{r}) = 2\ \vec{\Omega}$ (see Fig. 1). Note that $\vec{f}$ is fixed but its components in some coordinate system (spherical coordinates for instance) can vary with position. The minus sign on the left-hand side of (1) is so that PV is generally positive for gravitationally stable - low Rossby number flows in the northern hemisphere.

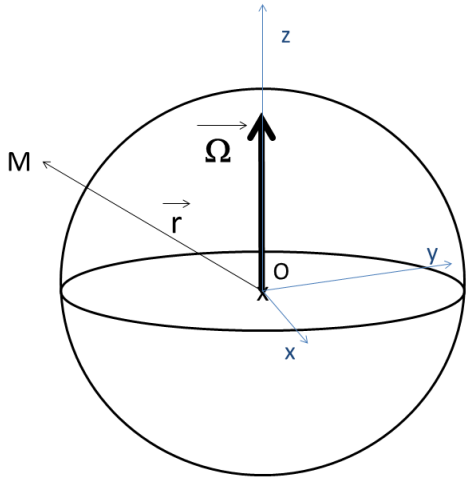

Figure 1: General Earth referential.

In the ocean, the Boussinesq approximation is typically valid and $\vec{\nabla}\rho/\rho$ can be replaced by $\vec{\nabla}\rho/\rho_0$, where ρ_0 is a mean oceanic density. ρ_0 can then be omitted from the definition of PV and we can use:

$$
\begin{aligned}
PV_{Ertel} &= -(\vec{\nabla} \times \vec{U} + \vec{f}).\vec{\nabla}\rho \\
&= -(\vec{\nabla} \times \vec{U}_a).\vec{\nabla}\rho
\end{aligned} \tag{2}
$$

We retain this definition for PV as it leads to clearer expressions for the calculations we present and the formulas we obtain. This approximation is however not necessary and all the following results are valid provided ρ is replaced by $G(\rho) = log(\rho)$ (see Appendix B).

2.2. Properties

2.2.1. Conservation

The non-hydrostatic Navier-Stokes equations (with Boussinesq approximation) are:

$$
\begin{aligned}
&\frac{d}{dt}\vec{U} + \vec{f} \times \vec{U} = -\frac{\vec{\nabla} P}{\rho_0} - \vec{g}\frac{\rho}{\rho_0} + \vec{F} \\
&div(\vec{U}) = 0 \\
&\frac{d}{dt}\rho = \dot{\rho}
\end{aligned} \tag{3}
$$

where $\vec{U} = (u, v, w)$ is the velocity field, $\frac{d}{dt}\phi = \partial_t\phi + \left(\vec{U}.\vec{\nabla}\right)\phi$, $\vec{f} = (0, f_y, f_z)$ is the Coriolis vector, P is the pressure, ρ is the potential density and $\vec{F} = (F_x, F_y, F_z)$ and $\dot{\rho}$ are terms associated with diabatic processes for momentum and density fields.

The Lagrangian evolution of Ertel PV can be derived from Eq. 3:

$$
\frac{d}{dt}PV_{Ertel} = -(\vec{\nabla} \times \vec{F}).\vec{\nabla}\rho - (\vec{\nabla} \times \vec{U} + \vec{f}).\vec{\nabla}\dot{\rho} \tag{4}
$$

As shown by Ertel (1942), PV_{Ertel} is thus conserved in regions where diabatic processes are negligible.

The evolution/conservation of PV following fluid particles is a major constraint for geophysical fluid dynamics (Hoskins et al., 1985). To study geophysical fluids, simplified forms of Eq. 3 are sought which conserve a simplified expression for PV (White et al., 2005). This is the case for instance for quasigeostrophic or primitive equations (Pedlosky, 1987; Cushman-Roisin and Beckers, 2011; McWilliams, 2006). For the primitive equations, the hydrostatic approximation is assumed and f_y is neglected, PV can be written (White et al., 2005):

$$PV_{PE} = -(\partial_x v - \partial_y u + f_z)\ \partial_z \rho + \partial_z v\ \partial_x \rho - \partial_z u\ \partial_y \rho \tag{5}$$

where f_z is the (local) vertical component of the Coriolis vector and is called Coriolis parameter.

The Lagrangian conservation of PV_{PE} is more conveniently derived, and achieved in numerical models, using density ρ instead of the geopotential vertical coordinate z. This has been one of the motivation for the development of isopycnic coordinate ocean models (see for instance Bleck et al., 1992; Hallberg, 1997). Using isopycnic coordinate, PV_{PE} can be written (Cushman-Roisin and Beckers, 2011):

$$PV_{PE} = \frac{\zeta + f_z}{h} \tag{6}$$

where $\zeta = (\partial_x v - \partial_y u)\ |_\rho$ is the relative vorticity, now calculated using horizontal velocity components along isopycnic surfaces and $h = -\partial_\rho z$ is a measure of the local stratification. We will see below how the expression of

PV can be easily derived in isopycnic coordinates for the full Navier-Stokes equations (including terms coming from all components of the Coriolis vector and non-hydrostatic effects).

2.2.2. Inversion

If (cyclo)geostrophy is assumed, the velocity field and stratification can be calculated from the PV and are associated with the balanced dynamics (Hoskins et al., 1985; Davis and Emanuel, 1991; McIntyre and Norton, 2000; Morel and McWilliams, 2001; Herbette et al., 2003, 2005). The PV of a fluid at rest and with a horizontally homogeneous stratification is not null. The potential vorticity anomaly (PVA) is defined as the difference between total PV and a reference PV associated with a state of rest of the entire fluid:

$$PVA = PV - \overline{PV}^{rest} \tag{7}$$

PVA is the part of the PV that is linked to the balanced dynamics and, at first order, it corresponds to the quasigeostrophic PV (Davis and Emanuel, 1991; McIntyre and Norton, 2000; Herbette et al., 2003).

The PV of the state at rest is given by the stratification at rest:

$$\overline{PV}^{rest} = -\vec{f}.\vec{\nabla}\overline{\rho}\mid_{\rho} = -f_z\ \partial_z\rho\mid_{\rho} = -\frac{f_z}{\partial_\rho \overline{z}(\rho)} = \frac{f_z}{\overline{h}} \tag{8}$$

An important point is that in Eq. 7 PVA has to be calculated along surfaces of constant density. This is underlined by the $|_\rho$ symbol in Eq. 8, which is valid for both non-hydrostatic and primitive equations. The stratification at rest $\overline{\rho}$ is associated with the adiabatic rearrangement of the density to get a horizontally uniform field (Holliday and Mcintyre, 1981; Kang and Fringer,

2010) and it is generally not easy to determine. PVA is thus often used in idealised configurations where the fluid is at rest in some area (generally at the edge of the domain see sections 5.2 and 5.3 below). Alternatively, PVA can be associated with small scale processes, superposed on a larger scale circulation. The reference state can then be approximately determined as a spatial average (over a distance that is much larger than the processes scales).

3. Alternative expressions for PV

3.1. Divergence form

In the following, the calculations rely on general mathematical properties relating divergence, curl and gradient of 3D fields and integral properties of these operators, whose general forms are recalled in Appendix A.

Previous studies have shown that Ertel PV, as defined in Eq. 2, can be expressed in divergence form (see Schneider et al., 2003; Vallis, 2006). Trivial manipulations (explained in Appendix A, see Eq. A.1) lead to the following equivalent expressions for the PV in divergence form (remember $\vec{U}_a = \vec{U} + \vec{\Omega} \times \vec{r}$ is the absolute velocity, see Fig. 1):

$$PV_{Ertel} = -div(\vec{U}_a \times \vec{\nabla}\rho) \tag{9a}$$

$$= -div(\rho\ (\vec{\nabla} \times \vec{U}_a)) \tag{9b}$$

$$= -div(\vec{U} \times \vec{\nabla}\rho) - div(\rho\ \vec{f}). \tag{9c}$$

Notice that these expressions are exact, whatever the evolution (diabatic or adiabatic) of PV and have been reported and/or used before, in particular in atmospheric sciences (see Haynes and McIntyre, 1987; Bretherton and

Schar, 1993; Schneider et al., 2003; Vallis, 2006). Here we demonstrate that they also lead to consistent and convenient practical approach to calculating and analysing PV in ocean modelling.

3.2. Implication for the integral of PV

Using Ostrogradsky-Stokes theorem (see Appendix A), the previous divergence form of the PV simplifies the calculation of the integral of PV_{Ertel} over a volume V. It can be calculated from the knowledge of the density, velocity or relative vorticity fields around the surface ∂V containing V. Equations 9 give the exact expressions:

$$\int\int\int_V PV_{Ertel}\, dV = -\int\int_{\partial V} \rho\, (\vec{\nabla} \times \vec{U}_a).d\vec{S} \tag{10a}$$

$$= -\int\int_{\partial V} (\vec{U}_a \times \vec{\nabla}\rho).d\vec{S} \tag{10b}$$

$$= -\int\int_{\partial V} \rho\, \vec{f}.d\vec{S} - \int\int_{\partial V} (\vec{U} \times \vec{\nabla}\rho).d\vec{S}. \tag{10c}$$

The previous expressions follow from the definition of PV and do not depend on equations governing its evolution. They represent exact instantaneous diagnostics of net PV within a volume and should not be confused with the general flux form of the PV evolution equation (Haynes and McIntyre, 1987).

4. Applications to the calculation of PV

In this section, we discuss how the divergence formulation, and its associated integral constraints Eq. 10, yield an easier way to diagnose PV and maintain balances between volume integral of PV and boundary conditions (Eq. 10).

4.1. PV diagnostics for numerical models

The diagnosis of PV from numerical model outputs is generally cumbersome if the literal form (Eq. 2 or 5) is chosen as it implies numerous gradients calculated at different grid points, which then have to be averaged. The use of the divergence form simplifies the PV calculation and also preserves Eq. 10.

As they are used in the majority of ocean circulation models, we consider a 3D C-grid, which are 3D extensions of the horizontal Arakawa C-grid (see Fig. 2 and Arakawa and Lamb, 1977). Using Cartesian coordinates, we start from the divergence form of PV (9b) rewritten as:

$$\begin{aligned} PV_{Ertel} &= -div(\rho\ (\vec{\zeta}+\vec{f})) \\ &= -\partial_x(\rho(\zeta^x+f^x)) - \partial_y(\rho(\zeta^y+f^y)) - \partial_z(\rho(\zeta^z+f^z)) \end{aligned} \tag{11}$$

where $\vec{\zeta} = \vec{\nabla} \times \vec{U}$ and:

$$\begin{aligned} \zeta^x &= \partial_y w - \partial_z v \\ \zeta^y &= -\partial_x w + \partial_z u \\ \zeta^z &= \partial_x v - \partial_y u. \end{aligned} \tag{12}$$

The elementary cell for which PV is calculated has the density values at its corners (see Fig. 2). As is clear from Fig. 2, ζ^z values need to be calculated at the center of lower and upper sides of the cell. It can be calculated using the circulation along edges of the cell lower and upper sides. An interesting property of 3D C-grid is that this is straightforward, thanks to the position of the velocity points (located at the middle of edges parallel

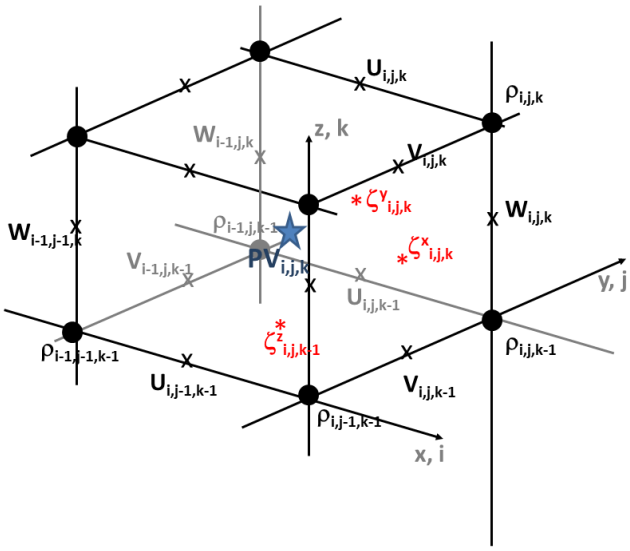

Figure 2: Elementary cell, for a 3D C-grid, used for the calculation of PV. We consider Cartesian coordinates $(x,\ y,\ z)$ associated with indices $(i,\ j,\ k)$.

to the velocity component). Density is averaged over the 4 density points located at the side corners. The same calculation is also valid for the other sides of the cell.

As a result, the PV of the cell can easily be calculated from physical fields within this single cell. We get:

$$\begin{aligned}
\zeta^x_{i,j,k} &= \frac{w_{i,j,k} - w_{i,j-1,k}}{\Delta y} - \frac{v_{i,j,k} - v_{i,j,k-1}}{\Delta z} \\
\zeta^y_{i,j,k} &= -\frac{w_{i,j,k} - w_{i-1,j,k}}{\Delta y} + \frac{u_{i,j,k} - u_{i,j,k-1}}{\Delta z} \\
\zeta^z_{i,j,k} &= \frac{v_{i,j,k} - v_{i-1,j,k}}{\Delta x} - \frac{u_{i,j,k} - u_{i,j-1,k}}{\Delta y},
\end{aligned} \tag{13}$$

and finally

$$\begin{aligned}
PV_{i,j,k} = & -\frac{\overline{\rho^x}_{i,j,k}(\zeta^x_{i,j,k} + f^x_{i,j,k}) - \overline{\rho^x}_{i-1,j,k}(\zeta^x_{i-1,j,k} + f^x_{i-1,j,k})}{\Delta x} \\
& -\frac{\overline{\rho^y}_{i,j,k}(\zeta^y_{i,j,k} + f^y_{i,j,k}) - \overline{\rho^y}_{i,j-1,k}(\zeta^y_{i,j-1,k} + f^y_{i,j-1,k})}{\Delta y} \\
& -\frac{\overline{\rho^z}_{i,j,k}(\zeta^z_{i,j,k} + f^z_{i,j,k}) - \overline{\rho^z}_{i,j,k-1}(\zeta^z_{i,j,k-1} + f^z_{i,j,k-1})}{\Delta z},
\end{aligned} \tag{14}$$

where

$$\overline{\rho^x}_{i,j,k} = 1/4(\rho_{i,j,k} + \rho_{i,j,k-1} + \rho_{i,j-1,k} + \rho_{i,j-1,k-1}) \tag{15}$$

is the density calculated at the position of $\zeta^x_{i,j,k}$ (see Fig. 2), and so forth for the other components. The Coriolis components $f^{x/y/z}_{i,j,k}$ are calculated at the location of the $\zeta^{x/y/z}_{i,j,k}$ points. Note that for the specific discretization of the 3D C-grid (see Fig. 2), the divergence form leads to a compact expression of PV : in Eq. 14 PV is calculated using density and velocity values from a single grid cell.

Equation 14 has a flux form, which ensures that, given a volume V, the integral of PV calculated over V using the accumulation of individual cells or using Eq. 10 exactly match, thus preserving the general balances between integral of PV and boundary conditions for any volume. Flux form PV expressions can be derived for B-grids or other grids, with a similar property.

4.2. General PV expression in isopycnal coordinates

The integral constraints 10 may be used for an easier derivation of the expression of PV in any coordinate systems and for the full Navier-Stokes equations. As an example, we calculate PV using the isopycnic coordinate ρ instead of the geopotential coordinate z (see section 4a of Schneider et al., 2003). This is of interest as the interpretation of the PV evolution, in particular the PV anomaly, has to be made along isopycnic surfaces (Hoskins et al., 1985).

For the sake of simplicity, we just replace the vertical Cartesian coordinate z by ρ and we keep the Cartesian (x, y) coordinates in the horizontal (see Fig. 3). Other systems (for instance spherical) can be used without much more complications. We also keep the orthogonal Cartesian elementary vectors $(\vec{i}, \vec{j}, \vec{k})$ associated with axis (Ox, Oy, Oz) (see Fig. 3) to express all vectors.

In this framework, $z = z(x, y, \rho)$ is the vertical position of isopycnic surfaces, and to calculate PV, we will use Eq. 10b, which only requires the evaluation of the density gradient $\vec{\nabla}\rho = \partial_x\rho\ \vec{i} + \partial_y\rho\ \vec{j} + \partial_z\rho\ \vec{k}$, but using the (x, y, ρ) coordinates. To do so, we use:

$$h = -\partial_\rho z = -1/\partial_z \rho$$

$$\partial_x z \mid_{y,\rho} = -h \ \partial_x \rho \mid_{y,z}$$

$$\partial_y z \mid_{x,\rho} = -h \ \partial_y \rho \mid_{x,z}$$

The density gradient is then given by:

$$\vec{\nabla}\rho = \frac{1}{h}[\partial_x z \ \vec{i} + \partial_y z \ \vec{j} - \vec{k}] \tag{16}$$

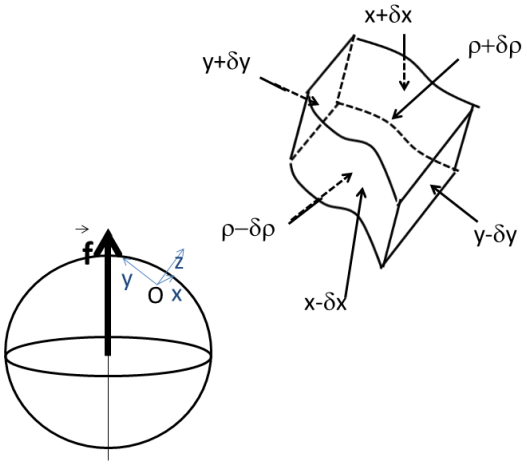

Figure 3: Coordinate system (x, y, ρ) and elementary volume and surfaces used to calculate PV_{Ertel} using the isopycnic coordinate.

Equation 10b is then applied to an elementary volume bounded by two isopycnic surfaces sketched in Fig. 3:

$$\int\int\int_{\delta V} PV_{Ertel}\ dV = -\int\int_{\partial\delta V} (\vec{U}_a \times \vec{\nabla}\rho).d\vec{S}$$
$$= -[(\vec{U}_a \times \vec{\nabla}\rho).d\vec{S}]_{\partial\delta V} \quad (17)$$

where $[.]_{\partial\delta V}$ is the flux through all surfaces delimiting δV. Note that $\vec{U}_a = u_a\ \vec{i} + v_a\ \vec{j} + w_a\ \vec{k}$ remains the absolute velocity field expressed in the orthogonal Cartesian system.

Since the flux across isopycnic surfaces ($\rho \pm \delta\rho$) is null and since the other surfaces are simple (vertical planes of constant y or x), Eq. 17 gives:

$$PV^{\rho}_{Ertel}\ \delta V = -\ [(\vec{U}_a \times \vec{\nabla}\rho).\vec{i}\ 2\delta y\ 2h\delta\rho]^{x+\delta x}_{x-\delta x}$$
$$-\ [(\vec{U}_a \times \vec{\nabla}\rho).\vec{j}\ 2\delta x\ 2h\delta\rho]^{y+\delta y}_{y-\delta y} \quad (18)$$

Given that $\delta V = 2\delta x\ 2\delta y\ 2\delta z = -2\delta x\ 2\delta y\ 2h\delta\rho$ and

$$\vec{U}_a \times \vec{\nabla}\rho = -\frac{1}{h}(v_a + w_a\partial_y z, -u_a - w_a\partial_x z, -u_a\partial_y z + v_a\partial_x z) \quad (19)$$

Eq. 18 gives:

$$PV^{\rho}_{Ertel} = \frac{\partial_x(v_a + w_a\partial_y z)\ |_\rho\ -\partial_y(u_a + w_a\partial_x z)\ |_\rho}{h}$$
$$= \frac{\partial_x(v + w\partial_y z)\ |_\rho\ -\partial_y(u + w\partial_x z)\ |_\rho\ + f_z - f_y\partial_y z}{h} \quad (20)$$

which is a generalised form of Eq. 6 with additional terms (in particular all components of the Coriolis effect). The terms $(u + w\partial_x z)\ |_\rho,\ (v + w\partial_y z)\ |_\rho$ represent the projection of the velocity field on the plane tangent to the isopycnic surface.

This exact general result can also be derived using Eq. 2, with a change of coordinate. But the calculations based on Eq. 10 offer a straightforward method.

4.3. Integration of PV in a "layer"

We consider a volume V constituted of a "layer" embedded between two isopycnic surfaces associated with densities ρ_1 and ρ_2, that can outcrop at the surface or bottom (see Fig. 4). The total PV contained within V may be deduced from Eq. 10c and trivial calculations (taking advantage of the fact that the boundaries ∂V of the layer are partly delimited by isentropic/isopycnic surfaces, and some rearrangements using Eq. A.4).

This leads to the following form, which depends only on physical fields at the surface and bottom outcropping regions:

$$\int\int\int_V PV_{Ertel}\ dV = -\int\int_{S^s+S^b+S^w} (\vec{U}\times\vec{\nabla}\rho).d\vec{S}$$
$$+\,[\int\int_{S^s} (\rho_1-\rho_s)\ d\vec{S} + \int\int_{S^b+S^w} (\rho_1-\rho_b)\ d\vec{S} + \int\int_{S^{\rho 2}} (\rho_1-\rho_2)\ d\vec{S}].\vec{f} \tag{21}$$

where $\rho_s(x,y)$ is the density at the ocean surface and $\rho_b(x,y)$ the density along the bottom of the ocean. This form takes advantage of the expression Eq. 10c to deal with volumes delimited by the two isopycnal surfaces S^{ρ_1} and S^{ρ_2}. Part of the layer boundaries are however associated with outcropping surfaces where density varies (S^s, S^w and S^b see Fig. 4). The first right hand side term of Eq. 21 depends on $\vec{U}\times\vec{\nabla}\rho$ and has to be evaluated along these surfaces. For this term, depending on the boundary condition used, it may be more convenient to switch back to a form in $\rho\,\vec{\zeta}$ like in Eq. 10a.

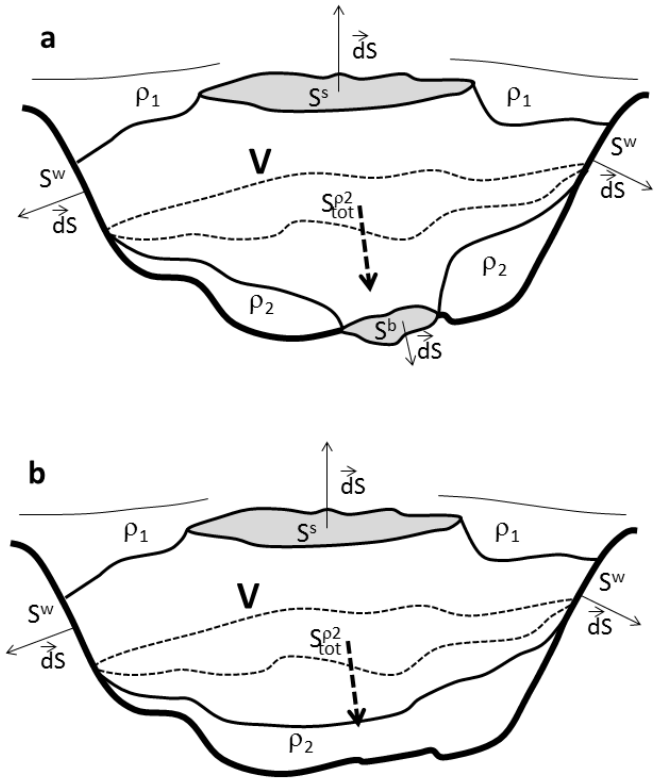

Figure 4: General shape of a layer, bounded by two isopycnic surfaces S^{ρ_1} and S^{ρ_2}, determining a volume where we integrate PV. Outcropping may occur at the surface (S^s) and at the bottom (S^b). As sketched in the upper plot (a) "Sidewalls" (S^w) and "Bottom" (S^b) surfaces are sometimes distinguished in numerical model. In this case, layers outcropping at the surface and sidewalls can have special constraints (b), as discussed in section 4.4.

This has to be done carefully using Eq. A.4 (see Appendix A). For instance we obtain for the surface S^s:

$$-\int\int_{S^s} (\vec{U} \times \vec{\nabla}\rho).d\vec{S} = \int\int_{S^s} (\rho_1 - \rho_s)\ \zeta_s\ dxdy \tag{22}$$

Finally, notice that the bottom surface has been divided in "Sidewalls" and "Bottom" regions (S^w and S^b, see Fig. 4), possibly associated with different boundary conditions. This is artificial if both surfaces are associated with the seafloor but we did make a difference for the sake of generality. For instance in academic configurations, such as a rectangular basin, boundary conditions at the walls and at the bottom can differ.

4.4. Impermeability theorem

The impermeability theorem (Haynes and McIntyre, 1987, 1990) states that there is no net transport of PV across isopycnic (or isentropic) surfaces, whatever the evolution. As already shown by Vallis (2006), Eq. 10b is a straightforward demonstration of this theorem. Indeed, across such surfaces, $d\vec{S}$ is parallel to $\vec{\nabla}\rho$ and Eq. 10b shows that they do not contribute to the calculation of the PV volume integral, whatever the evolution of the isopycnic surfaces. Thus, if there are no outcropping regions and the isopycnic surfaces are closed, the volume integral of Ertel PV within closed isopycnic surfaces is and remains null, whatever the evolution. Alternatively, modification of the volume integral of PV in an isopycnic layer is only possible when isopycnic surfaces outcrop (Haynes and McIntyre, 1987).

This principle can be slightly extended. Considering a layer without surface outcropping, and considering a no-slip boundary condition at the ocean bottom ($\vec{U}^w = \vec{U}^b = \vec{0}$), Eq. 21 gives:

$$\int\int\int_V PV_{Ertel}\ dV = [\ \int\int_{S^b+S^w} (\rho_1 - \rho_b)\ d\vec{S} + \int\int_{S^{\rho_2}} (\rho_1 - \rho_2)\ d\vec{S}\ ].\vec{f}. \quad (23)$$

If $\vec{U}^w = \vec{U}^b = \vec{0}$, the density distribution along the bottom can only be modified by diabatic (mixing) effects along the bottom. If the latter are negligible, the density field along the bottom is constant, and Eq. 23 then shows that there is no modification of the volume integral of PV. Indeed, in this case, both terms in the right hand side of Eq. 23 are constant. This is obvious for the first term. The second term is simply the scalar product of $\vec{f}$ (constant) and the net S^{ρ_2} surface vector. The latter only depends on the position of the edge of the surface, defined by the ρ_2 contour along the bottom, and thus constant too (an alternative way to demonstrate this is to transform the second term using Eq. A.4, see Appendix A). To conclude, with no-slip boundary conditions, the volume integral of PV is only modified if there exists mixing of the density near the bottom. In practice, the free-slip boundary condition is often preferred in ocean circulation models, the implication for the generation of PV will be discussed below (section 5.4).

Another case of interest is when outcropping only occurs at the surface and sidewalls (Fig. 4 b). In numerical models, sidewalls are sometimes considered vertical and the f_y component of the Coriolis vector is also neglected, so that $\vec{f}.d\vec{S} = 0$. If no-slip boundary conditions are used, many terms disappear in Eq. 21 and we then obtain:

$$\int\int\int_V PV_{Ertel}\ dV = -\int\int_{S^s} (\vec{U} \times \vec{\nabla}\rho)\ d\vec{S} + \int\int_{S^s} f_z(\rho_1 - \rho_s)\ dS \quad (24)$$

This draws attention to the potential importance of sloping boundaries and

the f_y component for the volume integral of PV at basin scale. It also shows that the surface terms in Eq. 24 are of special interest and we further evaluate their contributions in the next section.

5. Applications to specific balances

As discussed in the introduction, there exists a strong link between ocean circulation and the PV field, from mesoscale eddies to large scale currents. Equation 21 shows that there exists a balance between a volume integral of PV and boundary conditions. Using the divergence form of PV and the local PV calculation discussed in section 4.1 allows to preserve this balance. This is important for the physical interpretation of model outputs in terms of PV.

In this section, we illustrate how the balance can be used at several scales and for various processes in realistic or idealised configurations, for which some terms in Eq. 21 can be easily evaluated from observations (e.g. the surface ones), simplified or neglected (e.g. for no slip boundary conditions).

In section 5.1 we discuss how time variations of large scale volume integral of PV can be related to surface fields for both models and observations.

At mesoscale, surface density anomalies play a role similar to PVA (Bretherton, 1966). In sections 5.2 and 5.3 we show how Eq. 21 can be applied to isolated vortices and jets. We show that the balance leads to a precise relationship between surface density anomalies and PVA integrals, which has to be satisfied for isolated vortices and jets.

Finally, in section 5.4 we show how Eq. 21 can be applied to study the modification of PV in the bottom boundary layer, underlining the strong impact of the boundary conditions (free/no-slip).

5.1. Surface outcropping regions as indicators of the circulation of deep layers

For some choices of boundary conditions Eq. 21 reduces to Eq. 24. In addition, PV can be quickly modified by diabatic processes at the surface (Thomas, 2005; Morel et al., 2006; Thomas and Ferrari, 2008; Thomas et al., 2013; Wenegrat et al., 2018). We can thus hypothesise that the surface term:

$$I_{surf} = \int\int_{S^s} \left[(\rho_1 - \rho_s)\ \vec{f}\ -\ (\vec{U} \times \vec{\nabla}\rho_s)\right].d\vec{S}$$

dominates the time evolutions of the integral of PV within a deeper layer, which is itself linked to modification of the circulation (Rhines and Young, 1982a,b; Luyten et al., 1983; Holland et al., 1984; Rhines, 1986; Thomas and Rhines, 2002; Polton and Marshall, 2003; Deremble et al., 2014). Comparing I_{surf} from numerical models and observations is thus of interest.

Using $d\vec{S} = \vec{k}\ dxdy$ (where $\vec{k}$ is the vertical elementary vector), I_{surf} can be rewritten:

$$I_{surf} = \int\int_{S^s} \left[(\rho_1 - \rho_s)\ \vec{f}\ -\ (\vec{U} \times \vec{\nabla}\rho_s)\right].\vec{k}\ dxdy \tag{25}$$

Note that the integral in Eq. 25 only requires the knowledge of surface fields, in particular $(\vec{U} \times \vec{\nabla}\rho_s).\vec{k}$ only depends on the horizontal gradient of the surface density. I_{surf} can be calculated directly for numerical models. For observations, satellite observations (possibly complemented by in situ surface drifter observations) provide good estimates of the surface circulation over most of the ocean down to scales of order 25 km (see for instance Sudre and Morrow, 2008; Abernathey and Marshall, 2013; Rio et al., 2014). To do

so, the surface current is split into a geostrophic component and a component induced by the wind stress:

$$\vec{U}_s = \vec{U}_{geo} + \vec{U}_\tau \tag{26}$$

The geostrophic component $\vec{U}_{geo}$ and the associated relative vorticity can be calculated from the knowledge of the sea surface height (SSH) observed by satellite altimetry:

$$\vec{U}_{geo} = \frac{g}{f_z}\ \vec{k} \times \vec{\nabla} SSH \tag{27}$$

The wind induced surface current can be evaluated from satellite scatterometer observations and using the wind induced Ekman spiral which gives (see Cushman-Roisin and Beckers, 2011):

$$\vec{U}_\tau = \frac{\vec{\tau}_w^{-\pi/4}}{\sqrt{f_z \nu}} \tag{28}$$

where ν is the turbulent eddy viscosity and

$$\vec{\tau}_w^{-\pi/4} = \frac{\rho_a}{\rho_o} C_D \|W\| \vec{W}^{-\pi/4} \tag{29}$$

where $\vec{W}^{-\pi/4}$ is the surface wind but whose orientation has been rotated by $-\pi/4$, ρ_a/ρ_o is the ratio of the air to ocean density and $C_D \simeq 3.10^{-3}$ is the turbulent transfer parameter. As a result, the surface term contributing to the calculation of the observed PV within a layer (Eq. 25) can be written:

$$I_{surf} = \int\int_{S^s} (\rho_1 - \rho_s)\ f_z - [(\frac{g}{f_z}\ \vec{k} \times \vec{\nabla} SSH + \frac{\rho_a C_D \|W\| \vec{W}^{-\pi/4}}{\rho_o \sqrt{f_z \nu}}) \times \vec{\nabla} \rho_s].\vec{k}\ dxdy \tag{30}$$

and can be calculated from the observed sea surface density (calculated using SSS and SST from SMOS, Aquarius and microwave satellite observations), SSH and surface wind (all fields generally available over most of the ocean at $1/4^o$ resolution). We believe the comparison of I_{surf} from numerical models (Eq. 25) and from observations (Eq. 30) can provide an interesting new diagnostic for the validation of global or basin scale numerical models.

5.2. Constraints for coherent isolated vortices

Most observed eddies in the ocean are isolated[3] (Chelton et al., 2011). In QG and SQG models, for coherent isolated vortices, the volume integral of PVA and surface density field are linked (Morel and McWilliams, 1997; Assassi et al., 2016). We here extend this balance to Ertel PVA.

Consider a flat earth for which $\vec{f} = (0, 0, f_z)$ (f-plane approximation) and an axisymmetric vortex over a flat bottom (see Fig. 5 b-d). For the sake of simplicity, we also hypothesise that ρ is constant at the bottom and that $\overline{PV}^{rest}$ is spatially uniform (linear stratification at rest).

Integrating the PVA over the control volume V_o (see Fig. 5 b-d) gives:

$$\begin{aligned}\int\int\int_{V_o} PV A \; dV &= \int\int\int_{V_o} (PV_{Ertel} - \overline{PV}^{rest}) \; dV \\ &= \int\int\int_{V_o} (-\vec{f}.\vec{\nabla}\rho - \overline{PV}^{rest}) \; dV \\ &+ \int\int\int_{V_o} -(\vec{\nabla} \times \vec{U}).\vec{\nabla}\rho \; dV \end{aligned} \tag{31}$$

[3] An isolated vortex has a velocity field that decreases more rapidly than $1/r$, where r is the distance from its center, and the horizontal integral of its vorticity is null at any level.

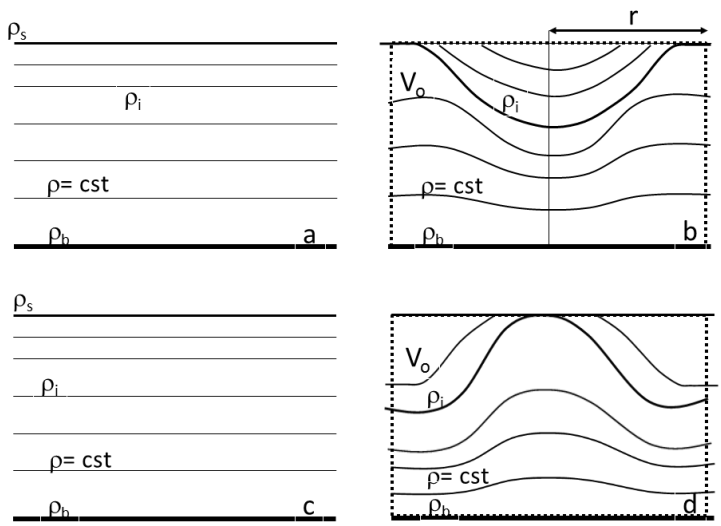

Figure 5: Vertical density structures for axisymmetric vortices having negative (b) and positive (d) surface anomalies. V_o (dashed contour) is the volume of integration and r is the distance form the vortex center. The background stratification at rest is indicated in panels a and c.

By using that $\overline{PV}^{rest} = -f_z(\rho_s^\infty - \rho_b)/H$, Eq. A.1b and the fact that the vortex is isolated, we get:

$$\int\int\int_{V_o} (-\vec{f}.\vec{\nabla}\rho - \overline{PV}^{rest})\ dV = -\int\int_{S^s} (\rho_s - \rho_s^\infty) f_z\ dx\ dy \tag{32}$$

and

$$\begin{aligned}\int\int\int_{V_o} -(\vec{\nabla}\times\vec{U}).\vec{\nabla}\rho\ dV &= -\int\int_{\partial V_o} \rho\ (\vec{\nabla}\times\vec{U}).d\vec{S} \\ &= -\int\int_{S^s} \rho_s\ \zeta_{surf}\ dx\ dy + O(\frac{1}{r}) \\ &= -\int\int_{S^s} (\rho_s - \rho_s^\infty)\zeta_{surf}\ dx\ dy + O(\frac{1}{r})\end{aligned} \tag{33}$$

where $\zeta_{surf} = \partial_x v - \partial_y u$ is the relative vorticity at the surface, ρ_s^∞ is the surface density at rest or the surface density far from the vortex center, and $(\rho_s - \rho_s^\infty)$ is the surface density anomaly associated with the vortex[4].

Integration of Eq. 31 over the whole (infinite) domain shows that PV anomalies associated with isolated vortices have to satisfy:

$$\int\int\int PV A\ dV\ +\ \int\int_{S^s} (\rho_s - \rho_s^\infty)(\zeta_{surf} + f_z)\ dx\ dy\ =\ 0 \tag{34}$$

This extends the integral constraints found in Assassi et al. (2016), which is

[4]In Eq. 33, the last line is obtained since $\int\int_{S^s} \zeta\ dx\ dy = 0$ for isolated vortices. The $O(1/r)$ term accounts for the integration over the bottom and lateral boundaries (dashed contours in Fig. 5). In particular, the lateral contribution scales as $\mid \rho\ H\ 2\pi\ r\ \partial_z U(r) \mid \leq O(1/r)$. The $O(1/r)$ rate of decrease is symbolic and the term simply indicates that these contributions vanish when $r \longrightarrow \infty$.

modified for strong surface vorticity (when $\mid \zeta_{surf} \mid \simeq f_z$) [5]. This is the case for submesoscale vortices (Lapeyre et al., 2006; Klein et al., 2008; Capet et al., 2008; Roullet et al., 2012; Gula et al., 2015; Molemaker et al., 2015; Capet et al., 2016).

Thus, for isolated vortices, a positive surface density anomaly is accompanied with negative PVA. A positive surface density is equivalent to a positive Dirac delta sheet of PVA (Bretherton, 1966). A similar constraint holds for a negative density anomaly. Hence, the generalised PVA structure of isolated vortices has both positive and negative values, which implies opposite sign PV gradient and opens the possibility of barotropic/baroclinic instabilities (Charney and Stern, 1962; Ripa, 1991). This has an impact on the evolution (stability and displacement) of the vortex (see Morel and McWilliams, 1997). In idealised studies dealing with the dynamics of isolated vortices, instability of the initial vortex structure can spoil the analysis and it is preferential to use specific methods, based on the inversion of stable PV structures, to initialise isolated vortices in models (see Herbette et al., 2003).

Moreover, the constraint Eq. 34 can have implications for methodologies deriving velocity fields of vortices from surface density observations. The methodologies empirically generate PVA distributions based on large-scale PV distributions or statistical correlations between surface density observations and PVA (Lapeyre et al., 2006; Lapeyre and Klein, 2006; Lapeyre, 2009; Ponte et al., 2013; Wang et al., 2013; Fresnay et al., 2018). In general,

[5] Strictly speaking, strong anticyclonic vortices, for which $\zeta_{surf} < -f_z$, could even reverse the sign of the deep PVA, but these structures are subject to inertial instability and are not long lived structures.

the derived PVA distributions do not satisfy constraint 34. The consequence is that the velocity field of a reconstructed vortex decreases slowly, which can lead to spurious calculations near lateral boundaries (the methodologies often consider periodic boundary conditions). It could be interesting to modify the methodologies so as to satisfy Eq. 34 in the vicinity of each vortex. We however have no clue on the spatial distribution of the PVA from the constraint (PVA poles, crown, vertically aligned or not, vertical position within the water column, possibly multiple poles of opposite sign, ...) and the reconstruction of the vertical vortex PVA have thus to be done carefully.

5.3. Constraints for jets and surface fronts

Similar constraints can be found for density fronts associated with jet-like currents. We consider a 2D configuration with no variation in the y direction. In 2D, Eq. 10 becomes

$$\begin{aligned}\int\int_S PV_{Ertel}\ dS &= -\int_{\partial S} \rho\ (\vec{\nabla}\times\vec{U}_a).\vec{n}\ dl \\ &= -\int_{\partial S} (\vec{U}_a\times\vec{\nabla\rho}).\vec{n}\ dl \\ &= -\int_{\partial S} \rho\ \vec{f}.\vec{n}\ dl - \int_{\partial S} (\vec{U}\times\vec{\nabla\rho}).\vec{n}\ dl \end{aligned} \tag{35}$$

Consider a 2D front outcropping at the surface but with a constant density along a flat bottom (see Fig. 6). The velocity field can be written $\vec{U} = \mathcal{V}(x,z)\ \vec{j}$, where $\mathcal{V}$ is the velocity component along the y axis. For jet-like currents the velocity vanishes away from the front: $\mathcal{V}(x \longrightarrow \pm\infty, z) = 0$. The stratification is different on both sides of the front and varies from $\bar{\rho}^{-\infty}(z)$ to $\bar{\rho}^{+\infty}(z)$.

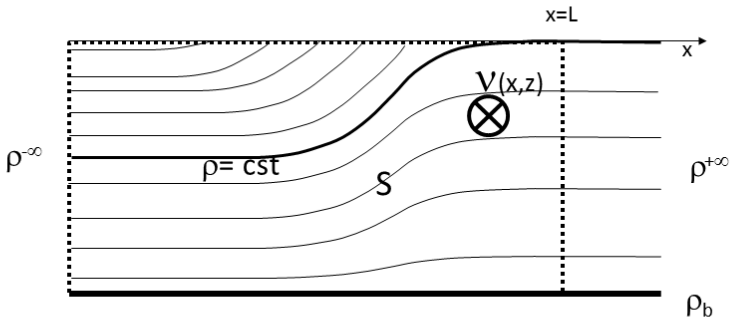

Figure 6: Vertical density structures for a surface outcropping front. S (dashed contour) is the surface of integration from $x = -\infty$ to $x = L$.

For this configuration, the determination of the reference PV, associated with the state at rest, is slightly more delicate, as we hypothesised that both the left and right edges of the front are at rest. It has however to be chosen at the left edge as only this side covers the entire density range. The reference PV is thus $PV_{rest}^{-\infty}$ and we then integrate PVA from $x = -\infty$ to $x = L$. Again, for the sake of simplification, we hypothesise that $\vec{f} = (0, 0, f_z)$ and $PV_{rest}^{-\infty}$ is spatially uniform. Trivial manipulations yield an equation similar to Eq. 33:

$$\begin{aligned}\int\int_S PV A \; dS &= \int\int_S PV_{Ertel} - PV_{rest}^{-\infty} \; dS \\ &= -\int_{-\infty}^{x=L} (\rho - \rho^{-\infty}) \mid_{z=0} \; (\zeta_z + f_z) \mid_{z=0} \; dx \\ &+ \int_{z=-H}^{z=0} (\partial_z \rho \; \mathcal{V}) \mid_{x=L} \; dz \end{aligned} \tag{36}$$

Assuming the velocity has a jet-like structure, $\mathcal{V}(x = L, z)$ becomes small enough so that the last term in Eq. 36, can be neglected. Given the density structure discussed here (see Fig. 6), $(\rho - \rho^{-\infty}) \mid_{z=0}$ is positive, which shows that a negative PVA must exist below the outcropping region for jets (if $(\zeta_z + f_z)$ remains positive). Opposite sign generalised PVA is necessarily associated with opposite sign PVA gradients and to instability (Charney and Stern, 1962). Similarly to isolated vortices, integral constraint 36 can be useful to study the instability of surface fronts and for methods aiming at reconstructing the ocean at mesoscale and submesoscale via an estimation of PVA within the water column (Lapeyre et al., 2006; Ponte et al., 2013; Spall, 1995; Boss et al., 1996; Manucharyan and Timmermans, 2013).

5.4. PV modification by bottom boundary layer processes

To study the modification of PV by -necessarily- diabatic processes, Eq. 4 complemented with the knowledge of diabatic terms is needed (Benthuysen and Thomas, 2012; Molemaker et al., 2015; Gula et al., 2015, 2019). However, as shown next, integral constraints may provide an interesting way to monitor the PV evolution within an isopycnic layer intersecting the topography.

To do so let us consider the development of a bottom boundary layer in 2D, with no variation in the y direction (Fig. 7).

We also consider that there is no outcropping at the surface and we follow a control area A_{2D} bounded by two isopycnic surfaces ρ_1 and ρ_2, the topography and a vertical boundary located at a distance L_∞ sufficiently large so that we can consider being away from the boundary layer and unaffected by the diabatic processes (the stratification and velocity field are unchanged, see Fig. 7). Integration of PV over this area gives (see Eq. 35):

$$\int\int_{A_{2D}} PV_{Ertel}\ dA = [\int_{S^w} (\rho_1 - \rho_b)\ \vec{n}\ dl + \int_{S^{\rho_2}} (\rho_1 - \rho_2)\ \vec{n}\ dl\ ].\vec{f} - \int_{S^w} (\vec{U} \times \vec{\nabla}\rho).\vec{n}\ dl - \int_{S^\infty} \mathcal{V}_\infty\ \partial_z \rho_\infty\ dz \qquad (37)$$

Given its definition, the last term in Eq. 37 does not vary.

The isopycnic levels initially intersect the topography at $x = 0$ and $x = L$, and along the topography the velocity field is $\mathcal{V}_o\ \vec{j}$ (Fig. 7a). After some diabatic processes, involving the viscous boundary layer and diapycnal mixing, the velocity profile and the position of isopycnic surfaces are modified. The positions of the intersection with the topography are now $x = L_1$ and $x = L_2$ and the velocity field along the topography is $\mathcal{V}\ \vec{j}$ (Fig. 7b). Some trivial manipulations give:

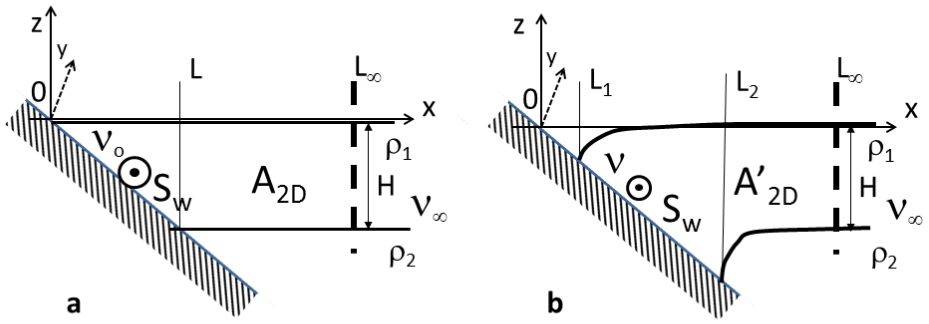

Figure 7: Vertical density structures in the deep ocean, near a topography. We consider a 2D configuration and we follow the evolution of a layer determined by two isopycnic levels ρ_1 and ρ_2 intersecting the topography. The initial velocity profile and the positions of the isopycnic levels (a) are modified by some diabatic processes (b).

$$\int_{S^w} (\rho_1 - \rho_b)\ \vec{n}.\vec{f}\ dl = -f_z \int_{L_1}^{L_2} (\rho_1 - \rho_b)\ dx$$
$$\int_{S^{\rho_2}} (\rho_1 - \rho_2)\ \vec{n}.\vec{f}\ dl = f_z\ (\rho_2 - \rho_1)\ (L_\infty - L_2)$$
$$-\int_{S^w} (\vec{U} \times \vec{\nabla}\rho).\vec{n}\ dl = -\int_{\rho_1}^{\rho_2} \mathcal{V}\ d\rho \tag{38}$$

Assuming a linear variation of the density along the bottom topography, this gives for the initial condition (see Fig. 7):

$$\int\int_{A_{2D}} PV_{Ertel}\ dA = f_z\ (\rho_2 - \rho_1)(L_\infty - \frac{L}{2}) - \overline{\mathcal{V}_o}\ (\rho_2 - \rho_1) - \int_{S^\infty} \mathcal{V}_\infty\ \partial_z \rho_\infty\ dz \tag{39}$$

and after the diabatic modification:

$$\int\int_{A'_{2D}} PV_{Ertel}\ dA = f_z\ (\rho_2 - \rho_1)(L_\infty - \frac{L_1 + L_2}{2}) - \overline{\mathcal{V}}\ (\rho_2 - \rho_1) - \int_{S^\infty} \mathcal{V}_\infty\ \partial_z \rho_\infty\ dz \tag{40}$$

where $\overline{\mathcal{V}}$ is the mean velocity along the bottom topography (where the average is weighted by density). The net modification of the volume integral of PV within the layer is thus:

$$\Delta \int\int_{layer} PV = -(\rho_2 - \rho_1)\ f_z\ \Delta X_{bot}^{\rho_1/\rho_2} - (\rho_2 - \rho_1)\ \Delta \mathcal{V}_{bot}^{\rho_1/\rho_2} \tag{41}$$

where $\Delta \mathcal{V}_{bot}^{\rho_1/\rho_2} = \overline{\mathcal{V}} - \overline{\mathcal{V}_o}$ is the modification of the mean velocity field along the bottom and within the layer ρ_1/ρ_2, and $\Delta X_{bot}^{\rho_1/\rho_2} = \frac{(L_1+L_2)-L}{2}$ is the modification of the mean x position of the layer along the bottom.

If no-slip conditions are chosen at the bottom, we recover that only density mixing along the bottom can modify the volume integral of PV within a layer, as already discussed in section 4.4. The time evolution of the volume integral of PV then only depends on the variation of the position of the intersection of the isopycnic layer: it is negative if the layer goes downslope (destratification case as illustrated in Fig. 7) and positive if the layer goes upslope (restratification case). Our results are qualitatively consistent with Benthuysen and Thomas (2012), despite the fact that we consider a layer and not a fixed box for the volume integral of PV.

Equation 41 allows the possibility to consider free-slip bottom conditions. Free-slip boundary conditions is the constraint usually used in numerical models and can provide an additional modification of the volume integral of PV if viscous effects are considered, as first imagined by D'Asaro (1988). These viscous effects have to be added to the effect of the modification of density studied in Benthuysen and Thomas (2012) and discussed above. Equation 41 shows that they superimpose when calculating the volume integral of PV and generally act similarly. Since our results are only diagnostics, we have to "imagine" the evolution of the velocity and density fields along the boundary to evaluate the possible PV modification. If we consider a velocity field with the shallow region on its right ($\overline{\mathcal{V}_o} < 0$, as depicted in Fig. 7), in the northern hemisphere, the bottom friction develops a downslope Ekman flux that leads to destratification and mixing induces a negative volume integral of PV variation. We can also assume that bottom friction also acts so as to reduce the strength of the velocity along the bottom topography, so that $\mid \overline{\mathcal{V}} \mid < \mid \overline{\mathcal{V}_o} \mid$. This leads to $\Delta\mathcal{V}_{bot}^{\rho_1/\rho_2} > 0$ and again to a negative volume integral of PV variation. Similarly an initial current with shallow region on its left would lead to a positive variation. This is consis-

tent with recent high resolution numerical results, using free-slip boundary conditions (see Molemaker et al., 2015; Gula et al., 2015; Vic et al., 2015; Gula et al., 2016, 2019) .

However, as discussed above, the important dynamical quantity is not necessarily the volume integral of PV. The key quantity is the PVA within an isopycnic layer. We can diagnose the mean PVA evolution within the boundary layer by dividing the volume integral of PV by the volume of the followed fluid (or its area A_{2D} and A'_{2D} in 2D, see Fig. 7). When all isopycnic surfaces remain parallel, this volume is constant (as is the case in Benthuysen and Thomas, 2012, for instance), the mean PVA is similar to the volume integral of PV and all previous results thus apply to the mean PVA. However, when this is not the case, the modification of PVA is more complex and also involves PV dilution or concentration within a layer which respectively gains or loses mass (see Haynes and McIntyre, 1990; Morel and McWilliams, 2001). This process is effective whenever there exists variation of turbulence along the topography, which is the case if the bottom slope or the velocity field vary spatially. In addition, global mass conservation requires that the depletion of one layer coincides with the inflation of another layer. Thus, differential diapycnal mixing in bottom boundary layers is probably ubiquitous in realistic configurations and we can expect the creation of both positive and negative PV anomalies.

6. Summary and discussion

6.1. Summary

In the present paper, we have used three different formulations of Ertel PV in divergence form (see Schneider et al., 2003, and Eq. 9) to calculate a

volume integral of PV from the knowledge of physical fields at the surface encompassing the volume. The divergence form and associated integral constraints have then been used to enable easier calculation of PV for numerical models, also preserving the balances between boundary conditions and PV. This has been explored in more details for specific physical processes at different scales.

We have also shown that the integral constraints associated with the divergence form lead to an easier calculation of the PV expression for non Cartesian coordinate systems. We have in particular illustrated this by calculating its expression in isopycnal coordinates for the general Navier-Stokes equations.

We have then considered the volume integral of PV within a "layer" delimited by two isopycnic surfaces and their intersections with the ocean surface and bottom. A general integral constraint was derived which allows to extend the PV impermeability theorem to no-slip conditions provided there is no density mixing along the topography. The integral constraint is then applied to several specific processes.

We first explored the link between volume integral of PV and surface fields at basin scale and we proposed an indicator to evaluate the time evolution of the volume integral of PV within a layer provided it outcrops at the sea surface (section 5.1). We proposed an indicator I_{surf}, depending on physical fields at the surface, as the signature of deeper PV. The indicator can be easily calculated for models and compared to observations (it depends on physical fields that can be estimated using satellite observations: wind, sea surface height, surface temperature and salinity).

When applied to isolated vortices or jets, given the equivalence between outcropping and surface PVA concentration (Bretherton, 1966), the balances

indicate that such structures have opposite sign generalised PVA and are thus potentially unstable. It also provides a useful constraint to estimate PVA structures from surface information as currently attempted empirically (Lapeyre et al., 2006; Lapeyre and Klein, 2006; Lapeyre, 2009; Ponte et al., 2013; Wang et al., 2013; Fresnay et al., 2018).

We finally applied the integral constraints to the modification of PV by diabatic processes within the bottom boundary layer. This provides a diagnostic of the PV evolution within a layer based on the displacement of its mean position and on the modification of the mean along slope velocity along the topography. It shows in particular that free-slip boundary conditions have potentially stronger effects on the formation of PVA in the viscous boundary layer. Differential mixing (variation of the density mixing along the topography) also leads to additional and possibly opposite sign PVA along the topography.

6.2. Discussion

Concerning the calculation of PV in numerical models, the divergence form approach can be adapted to any type of grid (including unstructured grids). In numerical models, the main problem is however Lagrangian conservation of PV during the (adiabatic) evolution of the flow. This principally relies on numerical schemes used in the model. There exists debates on the optimality of numerical grids (for instance between the Charney-Phillips grid and the 3D C-grid, see Arakawa and Moorthi, 1988; Bell, 2003) but a fair comparison relies on comparable numerical schemes too: numerical schemes have to be optimised for the conservation of PV for each grid (see Winther et al., 2007). When this is established, the influence of the PV diagnostic on the conservation property is interesting to assess too, even though this

influence is expected to be marginal compared to numerical schemes.

Concerning the I_{surf} indicator, we hypothesised that the time evolution of the integral of PV in a layer was mostly induced by the evolution of the surface fields. Recent studies (Ferrari et al., 2016; McDougall and Ferrari, 2017; de Lavergne et al., 2017; Callies and Ferrari, 2018) have however shown that mixing is bottom intensified at large scale and that it is associated with strong upwelling/downwelling circulations along the bottom topography which control the abyssal circulation overturning. According to what is discussed here in section 5.4, this can also modify the average PV. The signature of the modification of the deep PV on surface and bottom boundary terms of the PV balance (Eq. 21) can be tested using numerical models (Deremble et al., 2014). Equation 14 can be used to calculate PV consistently with Eq. 21.

An interesting perspective is to combine the present results with the water mass transformation (WMT) approach (Walin, 1982; Tziperman, 1986; Speer and Tziperman, 1992). If the surface contribution to the volume integral of PV can be exactly estimated for numerical models, we have to rely on geostrophic and Ekman currents for observations, so that we may miss some important ageostrophic contributions to the surface current, in particular associated with mixing. The WMT theory allows one to estimate the surface drift associated with mixing and heat fluxes and correct the surface observations where needed. The importance of this term for the PV balance can be assessed in models and the WMT approach provides a way to take this effect into account in observations.

Concerning the dynamics of isolated vortices and jets, the balances can be easily extended to take into account variations of density along the bottom (variations of bottom density have then to be included in Eq. 34 and

36) and a variable stratification at rest (see Eq. B.6 in Appendix B). This implies that the PVA evaluation is also possibly influenced by the bottom conditions, so that it may be difficult to reconstruct PVA profiles from the knowledge of surface density anomalies alone. Our calculations used the f-plane approximation. On the β-plane, weak vortices are dispersed into Rossby waves and their initial isolated nature can be rapidly lost. The results we derive here are thus of interest mainly for coherent vortices whose PV structures is comprised of closed PV contours. For these vortices, we can neglect the variation of the Coriolis parameter and Rossby waves.

Concerning modification of PV in the bottom boundary layer, the net modification of PV is also a function of time (Benthuysen and Thomas, 2013): the velocity and stratification in the bottom boundary layer do not reach instantaneously their equilibrium value (Benthuysen and Thomas, 2012). Thus, the final modification of PV along a boundary depends on the time a fluid parcel will remain in contact with the boundary layer. A Lagrangian perspective shows that 3D effects are important for realistic conditions: when a circulation encounters a bottom boundary, a fluid parcel will be in contact with the boundary layer for a limited time period which is a function of the boundary and circulation shapes (see Fig. 8). Both frictional effects and diapycnal mixing will modify the PV value of the fluid parcel and the strength of the created PVA which eventually separates from the boundary.

The identified processes for PV modification in the bottom boundary layer have physical grounds but their implementation in numerical simulations is a delicate issue as the result also depends on the choices of several parameters (turbulent viscosity and diffusion, but also numerical schemes, boundary conditions and closure schemes for momentum and tracers in the

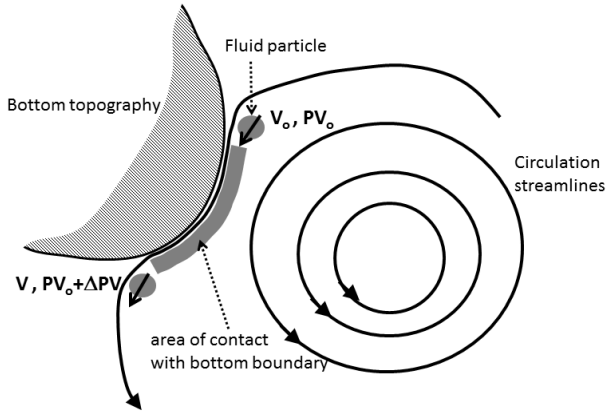

Figure 8: Schematic view of the modification of the PV of a fluid parcel that enters and exits a bottom boundary layer. The PV modification is a function of the time period the parcel remains within the bottom boundary layer, which is itself a function of the circulation and topography characteristics.

bottom boundary layer). Further studies are needed to evaluate the respective strength of each process in numerical simulations and in nature. The present results give exact diagnostics that can be helpful for that purpose.

Appendix A. General mathematical properties

For the sake of application to PV, we name $\vec{U}$, $\vec{\zeta}$ and ρ the fields used in the following equations, but the latter are exact general mathematical results whatever the meaning of the $\vec{U}$, $\vec{\zeta}$ and ρ fields.

First let us recall some basic properties for the divergence and curl of arbitrary fields:

$$div(\vec{U} \times \vec{B}) = (\vec{\nabla} \times \vec{U}).\vec{B} - (\vec{\nabla} \times \vec{B}).\vec{U}, \tag{A.1a}$$

$$div(\rho\ \vec{\zeta}) = \vec{\zeta}.\vec{\nabla}\rho + \rho\ div(\vec{\zeta}), \tag{A.1b}$$

$$\vec{\nabla} \times (\rho\ \vec{U}) = \rho\ (\vec{\nabla} \times \vec{U}) - \vec{U} \times \vec{\nabla}\rho, \tag{A.1c}$$

$$div(\vec{\nabla} \times \vec{U}) = 0, \tag{A.1d}$$

$$\vec{\nabla} \times (\vec{\nabla}\rho) = \vec{0}. \tag{A.1e}$$

Using $\vec{U} = \vec{U}_a$ and $\vec{B} = \vec{\nabla}\rho$ in A.1a, and $\vec{\zeta} = \vec{\nabla} \times \vec{U}_a$ in A.1b, Eq. A.1 allow to derive the divergence forms of the PV (Eq. 9).

We also use the Ostrogradsky-Stokes theorems for the integration of divergence and curl fields:

$$\int\int\int_V div(\vec{A})\ dV = \int\int_{\partial V} \vec{A}.d\vec{S} \tag{A.2}$$

and

$$\int\int_S (\vec{\nabla} \times \vec{A}).d\vec{S} = \int_{\partial S} \vec{A}.d\vec{l} \tag{A.3}$$

where V is a finite volume, ∂V is its external surface and $d\vec{S}$ is an elementary surface oriented outward and is perpendicular to $\partial\Omega$, S is a surface, ∂S is

its boundary and $d\vec{l}$ is an elementary line oriented parallel to ∂S and in the trigonometric direction when S is "seen from above" (see Fig. A.9).

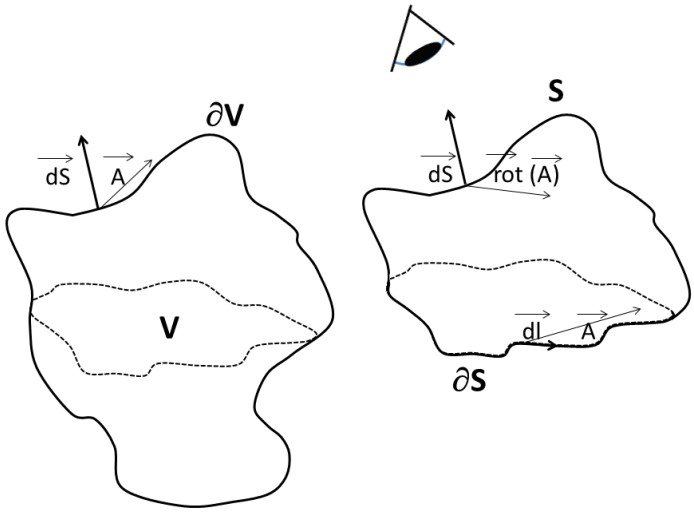

Figure A.9: Vector directions for the calculation of volume to surface to line integrals (Stokes theorem).

Finally, Eq. A.1 and A.3 also give:

$$\int\int_S \rho\ (\vec{\nabla} \times \vec{U}).d\vec{S} = \int\int_S (\vec{U} \times \vec{\nabla}\rho).d\vec{S} + \int_{\partial S} \rho\ \vec{U}.d\vec{l}. \qquad \text{(A.4)}$$

All these integral properties allow the derivation of Eq. 10 and its alternative forms.

Appendix B. Generalised constraints in nonuniform stratification

Appendix B.1. Generalised PV

The definition of PV (Eq. 2) could be changed and ρ can be replaced by $G(\rho)$ where G represents a general function. The generalised PV form is

thus:

$$\begin{aligned} PV_{Ertel-gen} &= -(\vec{\nabla} \times \vec{U} + \vec{f}).\vec{\nabla} G(\rho) \\ &= G'(\rho)\ PV_{Ertel} \end{aligned} \tag{B.1}$$

and such a change does not alter the basic properties associated with PV and discussed in the paper.

The integral of the generalised Ertel PV satisfies all results discussed above. In particular, Eq. 10 becomes:

$$\begin{aligned} \int\int\int_V PV_{Ertel-gen}\ dV &= -\int\int_{\partial V} G(\rho)\ (\vec{\nabla} \times \vec{U}_a).d\vec{S} \\ &= -\int\int_{\partial V} (\vec{U}_a \times \vec{\nabla} G(\rho)).d\vec{S} \\ &= -\int\int_{\partial V} G(\rho)\ \vec{f}.d\vec{S} - \int\int_{\partial V} (\vec{U} \times \vec{\nabla} G(\rho)).d\vec{S} \end{aligned} \tag{B.2}$$

The integration within a layer (Eq. 21) gives:

$$\begin{aligned} \int\int\int_V PV_{Ertel-gen}\ dV = \ [& \int\int_{S^s} (G(\rho_1) - G(\rho_s))\ d\vec{S} \\ & + \int\int_{S^b+S^w} (G(\rho_1) - G(\rho_b))\ d\vec{S} \\ & + \int\int_{S^{\rho_2}} (G(\rho_1) - G(\rho_2))\ d\vec{S}\ ].\vec{f} \\ & - \int\int_{S^s+S^b+S^w} (\vec{U} \times \vec{\nabla} G(\rho)).d\vec{S} \end{aligned} \tag{B.3}$$

Appendix B.2. Potential Vorticity Anomaly

For a fluid at rest, where the velocity field and vorticity are null and the stratification only depends on the vertical coordinate, the previous generalised form gives:

$$PV^{rest}_{Ertel-gen} = -G'(\overline{\rho})\ f_z\ \partial_z\overline{\rho}$$
$$= -f_z\ \partial_z[\ G(\overline{\rho}(z))\ ] \tag{B.4}$$

where f_z is the local vertical component of the Coriolis vector and $\overline{\rho}(z)$ is the reference profile of the stratification at rest. Choosing $G(X) = \bar{\rho}^{-1}(X)$, where $\bar{\rho}^{-1}$ is the inverse of the function $\bar{\rho}(z)$ (so that $G(\overline{\rho}(z)) = z$), yields $PV^{rest}_{Ertel-gen} = -f_z$: the reference PV is spatially uniform (f-plane approximation).

Using the generalised form of PV given in Eq. B.1 and B.4, we calculate the generalised PVA:

$$PVA_{gen} = PV_{Ertel-gen} - PV^{rest}_{Ertel-gen}$$
$$= -(\vec{\nabla} \times \vec{U} + \vec{f}).\vec{\nabla}G(\rho) + f_z \tag{B.5}$$

Since the stratification at rest is constant, the calculation performed in section 5.2 can be reproduced to lead to the general integral constraints for isolated vortices in a nonuniform stratification:

$$\int\int\int PVA_{gen}\ dV\ +\ \int\int_{S^s}\ (G(\rho) - G(\rho_s^\infty))(\zeta + f_z)\ dx\ dy\ =\ 0 \tag{B.6}$$

Note that $G = \bar{\rho}^{-1}$ is a monotonically increasing function, so that all the physics discussed in section 5.2 remains qualitatively valid.

Acknowledgements

Yves Morel is supported by the program "IDEX attractivity chairs" from Université de Toulouse (TEASAO project) and CNES (french space

agency; project TOSCA/OSTST "Alti-ETAO"). This work also benefited from the Copernicus Marine Environment Monitoring Service (CMEMS) DIMUP project. CMEMS is implemented by Mercator Ocean in the framework of a delegation agreement with the European Union. J. Gula benefited support from LEFE/IMAGO through the Project AO2017-994457-RADII. A. Ponte benefited support from CNES for his participation to the SWOT Science Team (project "New Dynamical Tools"). The authors acknowledge discussions with Prof. Peter Haynes (Chair holder of the TEASAO project) and Drs. Leif Thomas, Jef Polton and John Taylor which helped improving this manuscript. This work has been drastically improved thanks to the criticisms, comments and careful reading of anonymous reviewers and of Ocean Modelling editors. Their encouragements have also been a strong support for us and their suggestions led to a far better presentation of our results.

Bibliography

Abernathey, R. P., Marshall, J., 2013. Global surface eddy diffusivities derived from satellite altimetry. J. Geophys. Res.: Oceans 118 (2), 901–916.

Arakawa, A., Lamb, V., 1977. Computational design of the basic dynamical processes of the ucla general circulation model. Methods Comput. Phys. 17, 174–267.

Arakawa, A., Moorthi, S., 1988. Baroclinic instability in vertically discrete systems. J. Atmos. Sci. 45, 1688–1707.

Assassi, C., Morel, Y., Vandermeirsch, F., Chaigneau, A., Pegliasco, C., Morrow, R., Colas, F., Fleury, S., Carton, X., Klein, P., Cambra, R.,

2016. An index to distinguish surface and subsurface intensified vortices from surface observations. J. Phys. Oceanogr. 46, 2529–2552.

Bell, M. J., 2003. Conservation of potential vorticity on lorenz grids. Mon. Weather Rev. 131 (7), 1498–1501.

Benthuysen, J., Thomas, L., 2012. Friction and diapycnal mixing at a slope: Boundary control of potential vorticity. J. Phys. Oceanogr. 42, 1509–1523.

Benthuysen, J., Thomas, L., 2013. Nonlinear stratified spindown over a slope. J. Fluid Mech. 726, 371–403.

Bleck, R., Rooth, C., Hu, D., Smith, L., 1992. Salinity driven thermocline transients in a wind and thermohaline forced isopycnic coordinate model of the North Atlantic. J. Phys. Oceanogr. 22, 1486–1505.

Boss, E., Paldor, N., Thompson, L., 1996. Stability of a potential vorticity front; from quasi-geostrophy to shallow-water. J. Fluid Mech. 315, 65–84.

Bretherton, C., Schar, C., 1993. Flux of potential vorticity substance: A simple derivation and a uniqueness property. J. Atmos. Sci. 50 (12), 1834–1836.

Bretherton, F., 1966. Critical layer instability in baroclinic flows. Q.J.R. Meteorol. Soc. 92 (2), 325–334.

Callies, J., Ferrari, R., 2018. Dynamics of an abyssal circulation driven by bottom-intensified mixing on slopes. J. Phys. Oceanogr.

Capet, X., McWilliams, J. C., Molemaker, M. J., Shchepetkin, A. F., 2008. Mesoscale to submesoscale transition in the California Current sys-

tem. part i: Flow structure, eddy flux, and observational tests. J. Phys. Oceanogr. 38 (1), 29–43.

Capet, X., Roullet, G., Klein, P., Maze, G., 2016. Intensification of upper-Ocean submesoscale turbulence through charney baroclinic instability. J. Phys. Oceanogr. 46 (11), 3365–3384.

Charney, J., Stern, M., 1962. On the stability of internal baroclinic jets in a rotating atmosphere. J. Atmos. Sci. 19 (2), 159–172.

Chelton, D. B., Schlax, M. G., Samelson, R. M., 2011. Global observations of nonlinear mesoscale eddies. Progress in Oceanography 91 (2), 167 – 216.

Cushman-Roisin, B., Beckers, J.-M., 2011. Introduction to Geophysical Fluid Dynamics. Academic press, 875 pp.

Czaja, A., Hausmann, U., 2009. Observations of entry and exit of potential vorticity at the sea surface. J. Phys. Oceanogr. 39, 2280–2294.

D'Asaro, E., 1988. Generation of submesoscale vortices: A new mechanism. J. Geophys. Res.:Oceans 93-C6, 2156–2202.

Davis, C. A., Emanuel, K. A., 1991. Potential vorticity diagnostics of cyclogenesis. Mon. Weather Rev. 119 (8), 1929–1953.

de Lavergne, C., Madec, G., Roquet, F., Holmes, R. M., McDougall, T. J., 2017. Abyssal Ocean overturning shaped by seafloor distribution. Nature 551, 181.

Deremble, B., Wienders, N., Dewar, W. K., 2014. Potential vorticity budgets in the North Atlantic Ocean. J. Phys. Oceanogr. 44 (1), 164–178.

Ertel, H., 1942. On hydrodynamic eddy theorems. Physikalische Zeitschrift 43, 526–529.

Ferrari, R., Mashayek, A., McDougall, T. J., Nikurashin, M., Campin, J.-M., 2016. Turning Ocean mixing upside down. J. Phys. Oceanogr. 46 (7), 2239–2261.

Fresnay, S., Ponte, A. L., Le Gentil, S., Le Sommer, J., 2018. Reconstruction of the 3-d dynamics from surface variables in a high-resolution simulation of North atlantic. J. Geophys. Res.: Oceans 123 (3), 1612–1630.

Giordani, H., Lebeaupin Brossier, C., Léger, F., Caniaux, G., 2017. A pv-approach for dense water formation along fronts: Application to the Northwestern mediterranean. J. Geophys. Res.: Oceans 122 (2), 995–1015. URL http://dx.doi.org/10.1002/2016JC012019

Gula, J., Blacic, T. M., Todd, R. E., 2019. Submesoscale Coherent Vortices in the Gulf Stream. Geophys. Res. Lett. 46.

Gula, J., Molemaker, M., McWilliams, J., 2015. Topographic vorticity generation, submesoscale instability and vortex street formation in the Gulf Stream. Geophys. Res. Lett. 42, 40544062.

Gula, J., Molemaker, M., McWilliams, J., 2016. Topographic generation of submesoscale centrifugal instability and energy dissipation. Nature Communications 7, 12811.

Hallberg, R., 1997. Stable split time stepping schemes for large-scale Ocean modeling. J. Comp. Phys. 135, 54–65.

Hallberg, R., Rhines, P., 1996. Buoyancy-driven circulation in an Ocean

basin with isopycnals intersecting the sloping boundary. J. Phys. Oceanogr. 26 (6), 913–940.

Hallberg, R., Rhines, P., 2000. Boundary sources of potential vorticity in geophysical circulations. Developments in Geophysical Turbulence, R. M. Kerr and Y. Kimura, Eds., Kluwer Ac- ademic, 51–65.

Haynes, P., McIntyre, M., 1987. On the evolution of vorticity and potential vorticity in the presence of diabatic heating and frictional or other forces. J. Atmos. Sci. 44 (5), 828–841.

Haynes, P., McIntyre, M., 1990. On the conservation and impermeability theorems for potential vorticity. J. Atmos. Sci. 47 (16), 2021–2031.

Held, I., Pierrehumbert, R., Garner, S., Swanson, K., 1995. Surface quasi-geostrophic dynamics. J. Fluid Mech. 282, 1–20.

Herbette, S., Morel, Y., Arhan, M., 2003. Erosion of a surface vortex by a seamount. J. Phys. Oceanogr. 33, 1664–1679.

Herbette, S., Morel, Y., Arhan, M., Nov. 2005. Erosion of a surface vortex by a seamount on the beta plane. J. Phys. Oceanogr. 35 (11), 2012–2030.

Holland, W. R., Keffer, T., Rhines, P., 1984. Dynamics of the Ocean ic general circulation: The potential vorticity field. Nature 308, 698–705.

Holliday, D., Mcintyre, M. E., 1981. On potential energy density in an in-compressible, stratified fluid. J. Fluid Mech. 107, 221225.

Hoskins, B. J., McIntyre, M. E., Robertson, A. W., 1985. On the use and significance of isentropic potential vorticity maps. Q. J. Roy. Met. Soc. 470, 877–946.

Kang, D., Fringer, O., 2010. On the calculation of available potential energy in internal wave fields. J. Phys. Oceanogr. 40 (11), 2539–2545.

Klein, P., Hua, B. L., Lapeyre, G., Capet, X., Gentil, S. L., Sasaki, H., 2008. Upper Ocean turbulence from high-resolution 3d simulations. J. Phys. Oceanogr. 38 (8), 1748–1763.

Lapeyre, G., 2009. What vertical mode does the altimeter reflect? on the decomposition in baroclinic modes and on a surface-trapped mode. J. Phys. Oceanogr. 39 (11), 2857–2874.

Lapeyre, G., 2017. Surface quasi-geostrophy. Fluids 2 (1).

Lapeyre, G., Klein, P., 2006. Dynamics of the upper Oceanic layers in terms of surface quasigeostrophy theory. J. Phys. Oceanogr. 36, 165–176.

Lapeyre, G., Klein, P., Hua, B., 2006. Oceanic restratification forced by surface frontogenesis. J. Phys. Oceanogr. 36 (8), 1577–1590.

Luyten, J. R., Pedlosky, J., Stommel, H., 1983. The ventilated thermocline. J. Phys. Oceanogr. 13 (2), 292–309.

Manucharyan, G., Timmermans, M.-L., 2013. Generation and separation of mesoscale eddies from surface Ocean fronts. J. Phys. Oceanogr. 43 (12), 2545–2562.

Marshall, J., Nurser, G., 1992. Fluid dynamics of Ocean ic thermocline ventilation. J. Phys. Oceanogr. 22, 583–595.

McDougall, T. J., Ferrari, R., 2017. Abyssal upwelling and downwelling driven by near-boundary mixing. J. Phys. Oceanogr. 47 (2), 261–283.

McIntyre, M. E., Norton, W., 2000. Potential vorticity inversion on a hemisphere. J. Atmos. Sci. 57, 1214–1235.

McWilliams, J., 2006. Fundamentals of Geophysical Fluid Dynamics. Cambridge University Press.

McWilliams, J., Flierl, G., 1979. Evolution of isolated, non-linear vortices. J. Phys. Oceanogr. 9 (6), 1155–1182.

McWilliams, J. C., 1984. The emergence of isolated coherent vortices in turbulent flow. J. Fluid Mech. 146, 2143.

Meunier, T., Rossi, V., Morel, Y., Carton, X., 2010. Influence of bottom topography on an upwelling current: Generation of long trapped filaments. Ocean Modell. 41, 277–303.

Molemaker, M. J., McWilliams, J. C., Dewar, W. K., 2015. Submesoscale instability and generation of mesoscale anticyclones near a separation of the California Undercurrent. J. Phys. Oceanogr. 45 (3), 613–629.

Morel, Y., Darr, D., Tailandier, C., 2006. Possible sources driving the potential vorticity structure and long-wave instability of coastal upwelling and downwelling currents. J. Phys. Ocean . 36, 875–896.

Morel, Y., McWilliams, J., May 1997. Evolution of isolated interior vortices in the Ocean. J. Phys. Ocean . 27 (5), 727–748.

Morel, Y., McWilliams, J., 2001. Effects of isopycnal and diapycnal mixing on the stability of Ocean ic currents. J. Phys. Ocean . 31, 2280–2296.

Morel, Y., Thomas, L., 2009. Ekman drift and vortical structures. Ocean Modell. 27, 185–197.

Pedlosky, J., 1987. Geophys. Fluid Dyn. Springer, New York, 710 pp.

Polton, J., Marshall, D., 2003. Understanding the structure of the subtropical thermocline. J. Phys. Oceanogr. 33 (6), 1240–1249.

Ponte, A., Klein, P., Capet, X., Traon, P. L., Chapron, B., Lherminier, P., 2013. Diagnosing surface mixed layer dynamics from high-resolution satellite observations: Numerical insights. J. Phys. Oceanogr. 43 (7), 1345–1355.

Rhines, P., 1986. Vorticity dynamics of the Ocean ic general circulation. Annual review of Fluid Mechanics 18, 433–497.

Rhines, P., Young, W., 1982a. Homogenization of potential vorticity in planetary gyres. J. Fluid Mech. 122, 347–367.

Rhines, P., Young, W., 1982b. A theory of the wind-driven circulation. i, mid-Ocean gyres. J. Mar. Res. 40, 559–596.

Rio, M., Mulet, S., Picot, N., 2014. Beyond GOCE for the Ocean circulation estimate: Synergetic use of altimetry, gravimetry, and in situ data provides new insight into geostrophic and ekman currents. Geophys. Res. Lett. 41 (24), 8918–8925.

Ripa, P., 1991. General stability conditions for a multi-layer model. J. Fluid Mech. 222, 119–137.

Rossi, V., Morel, Y., Garcon, V., 2010. Effect of the wind on the shelf dynamics: formation of a secondary upwelling along the continental margin. Ocean Modell. 31, 51–79.

Roullet, G., McWilliams, J. C., Capet, X., Molemaker, M. J., 2012. Properties of steady geostrophic turbulence with isopycnal outcropping. J. Phys. Oceanogr. 42 (1), 18–38.

Schneider, T., Held, I., Garner, S., 2003. Boundary effects in potential vorticity dynamics. J. Atmos. Sci. 60 (8), 1024–1040.

Spall, M., 1995. Frontogenesis, subduction, and cross-front exchange at upper Ocean fronts. J. Geophys. Res. 100, 2543–2557.

Speer, K., Tziperman, E., 1992. Rates of water mass formation in the North Atlantic Ocean. J. Phys. Oceanogr. 22 (1), 93–104.

Sudre, J., Morrow, R. A., 2008. Global surface currents: a high-resolution product for investigating Ocean dynamics. Ocean Dynamics 58 (2), 101.

Sutyrin, G., Flierl, G., 1994. Intense vortex motion on the beta-plane - Development of the beta-gyres. J. Atmos. Sci. 51 (5), 773–790.

Talley, L. D., 1988. Potential vorticity distribution in the North Pacific. J. Phys. Oceanogr. 18 (1), 89–106.

Taylor, J., Ferrari, R., 2010. Buoyancy and wind-driven convection at mixed layer density fronts. J. Phys. Oceanogr. 40, 1222–1242.

Thomas, L., Ferrari, R., 2008. Friction, frontogenesis, and the stratification of the surface mixed layer. J. Phys. Oceanogr. 38 (11), 2501–2518.

Thomas, L., Rhines, P., 2002. Nonlinear stratified spin-up. J. Fluid Mech. 473, 211–244.

Thomas, L., Taylor, J., Ferrari, R., 2013. Symmetric instability in the Gulf Stream. Deep-Sea Res. 91, 96–110.

Thomas, L. N., 2005. Destruction of potential vorticity by winds. J. Phys. Oceanogr. 35 (12), 2457–2466.

Tziperman, E., 1986. On the role of interior mixing and air-sea fluxes in determining the stratification and circulation of the Ocean s. J. Phys. Oceanogr. 16 (4), 680–693.

Vallis, G. K., 2006. Atmospheric and Ocean ic Fluid Dynamics. Cambridge University Press, Cambridge, U.K.

Vic, C., Roullet, G., Capet, X., Carton, X., Molemaker, M. J., Gula, J., 2015. Eddy-topography interactions and the fate of the Persian Gulf Outflow. J. Geophys. Res.: Oceans 120 (10), 6700–6717.
URL http://dx.doi.org/10.1002/2015JC011033

Walin, G., 1982. On the relation between seasurface heat flow and thermal circulation in the Ocean. Tellus 34 (2), 187–195.

Wang, J., Flierl, G. R., LaCasce, J. H., McClean, J. L., Mahadevan, A., 2013. Reconstructing the Ocean 's interior from surface data. J. Phys. Oceanogr. 43 (8), 1611–1626.

Wenegrat, J. O., Thomas, L. N., Gula, J., McWilliams, J. C., 2018. Effects of the submesoscale on the potential vorticity budget of Ocean Mode Waters. J. Phys. Oceanogr. 48 (9), 2141–2165.

White, A. A., Hoskins, B. J., Roulstone, I., Staniforth, A., 2005. Consistent approximate models of the global atmosphere: shallow, deep, hydrostatic, quasihydrostatic and nonhydrostatic. Q. J. Roy. Met. Soc. 131 (609), 2081–2107.

Winther, N., Morel, Y., Evensen, G., 2007. Efficiency of high order numerical schemes for momentum advection. J. Mar. Sys. 67, 31–46.

Highlights

- Ertel potential vorticity (PV) expressions in divergence form improve PV diagnostics in models.
- Balances are derived between volume integral of PV and boundary conditions.
- Practical numerical computations of PV, preserving balances, are proposed.
- The implications of balances are examined for selected processes.

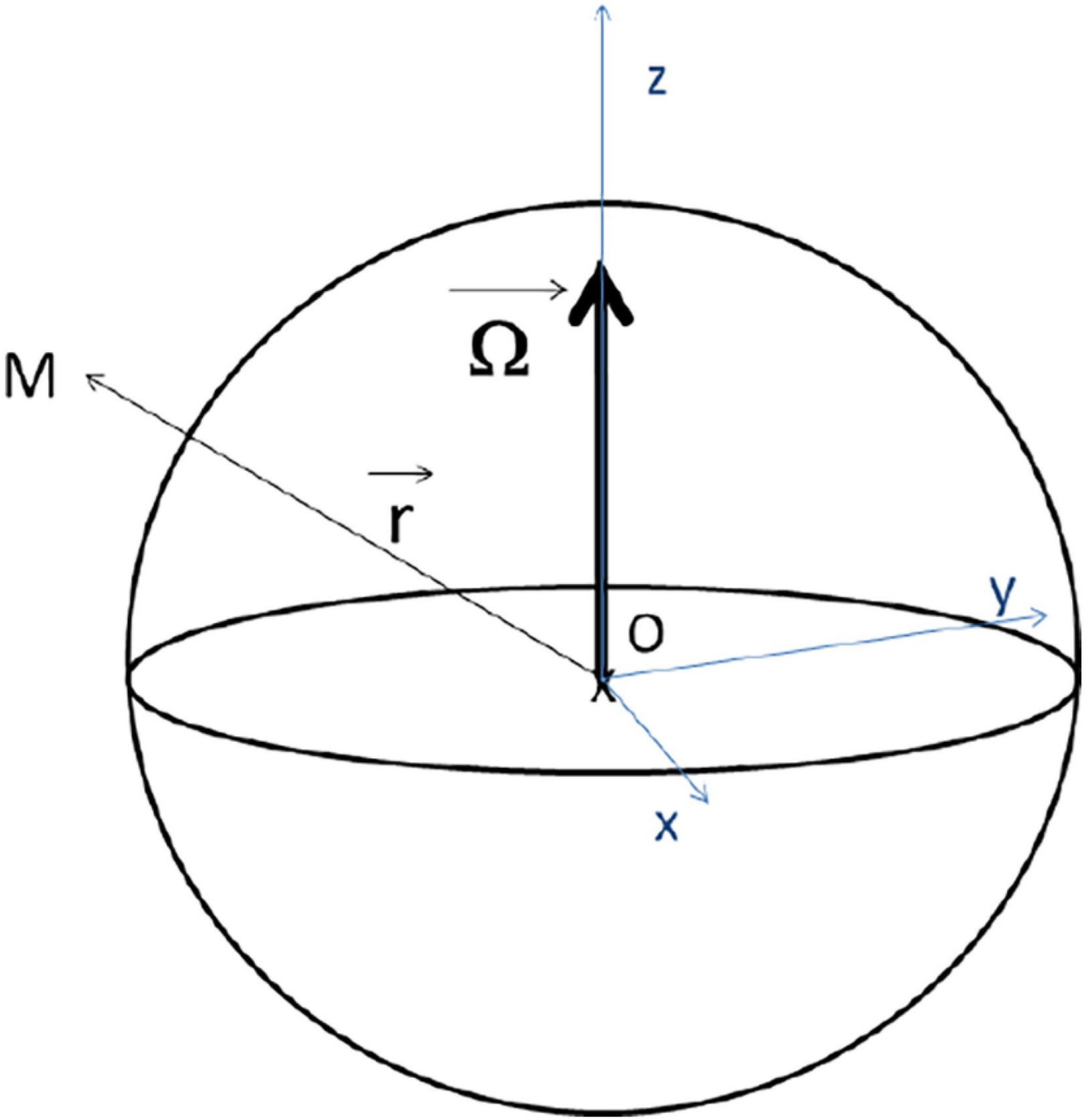

Figure 1

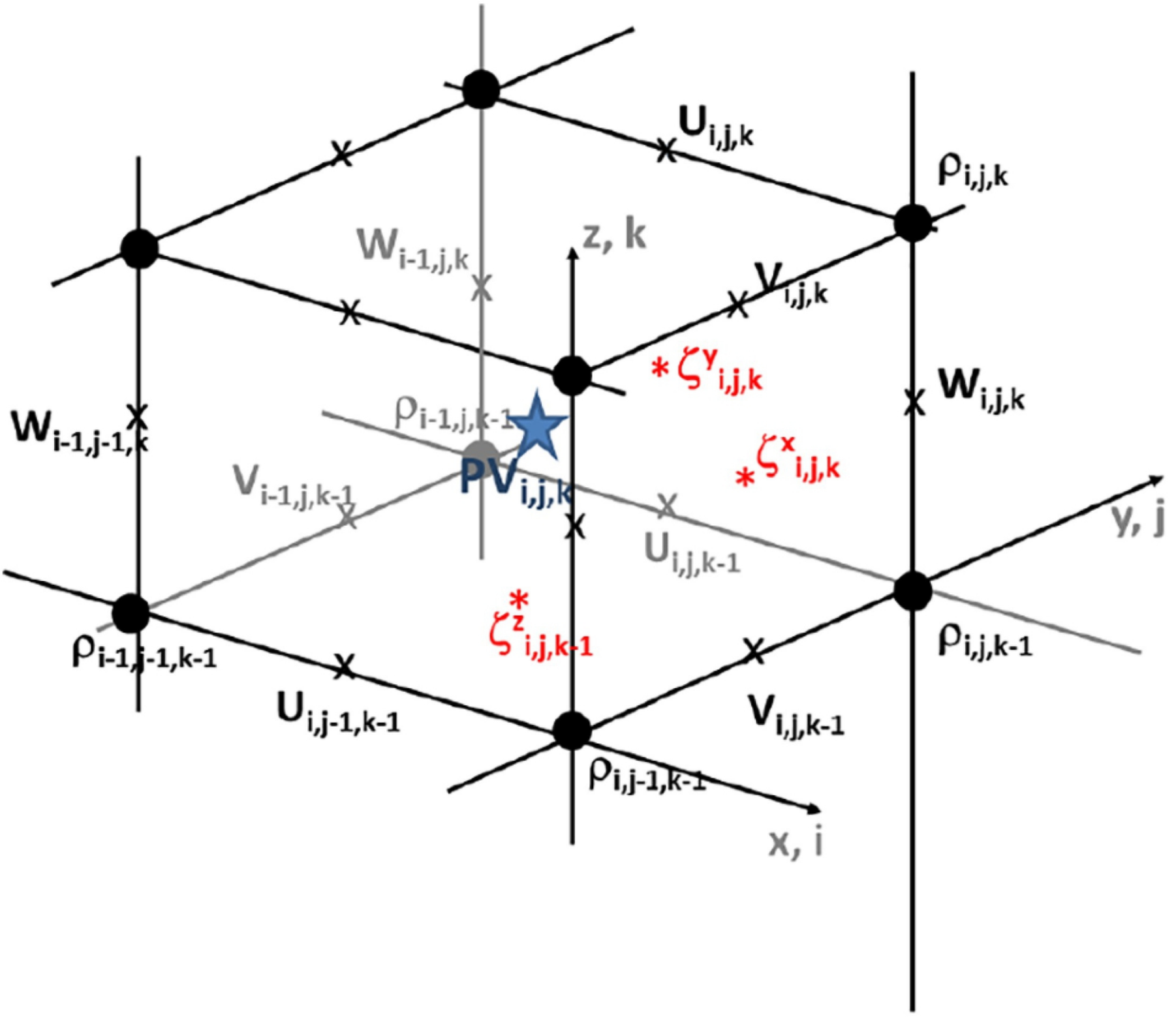
$U_{i,j,k}$
$\rho_{i,j,k}$
$W_{i-1,j,k}$
z, k
$V_{i,j,k}$
$*\zeta^{y}_{i,j,k}$
$W_{i,j,k}$
$\rho_{i-1,j,k-1}$
$W_{i-1,j-1,k}$
$*\zeta^{x}_{i,j,k}$
$V_{i-1,j,k-1}$
$PV_{i,j,k}$
y, j
$U_{i,j,k-1}$
$\zeta^{*z}_{i,j,k-1}$
$\rho_{i-1,j-1,k-1}$
$\rho_{i,j,k-1}$
$U_{i,j-1,k-1}$
$V_{i,j,k-1}$
$\rho_{i,j-1,k-1}$
x, i

Figure 2

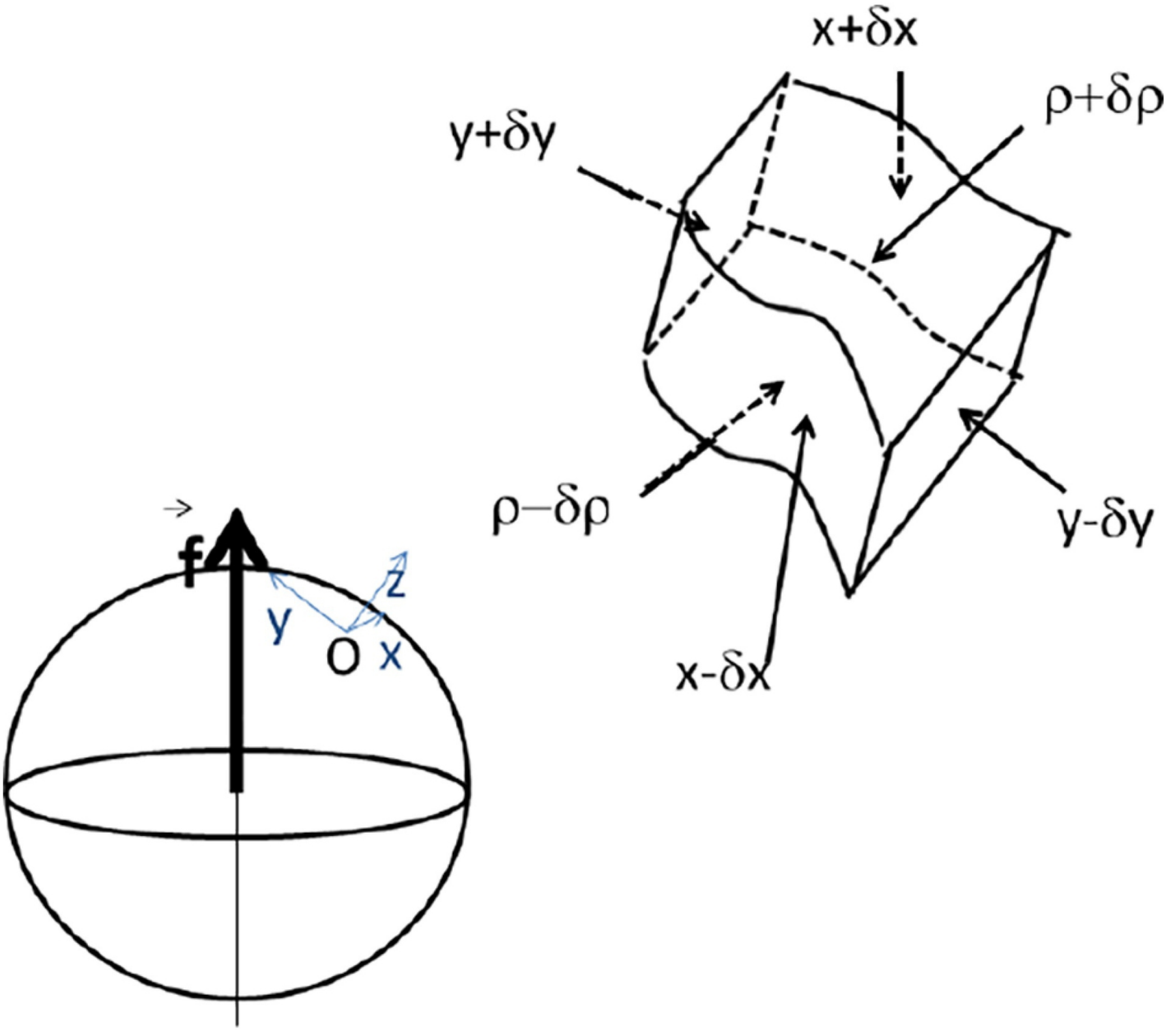

Figure 3

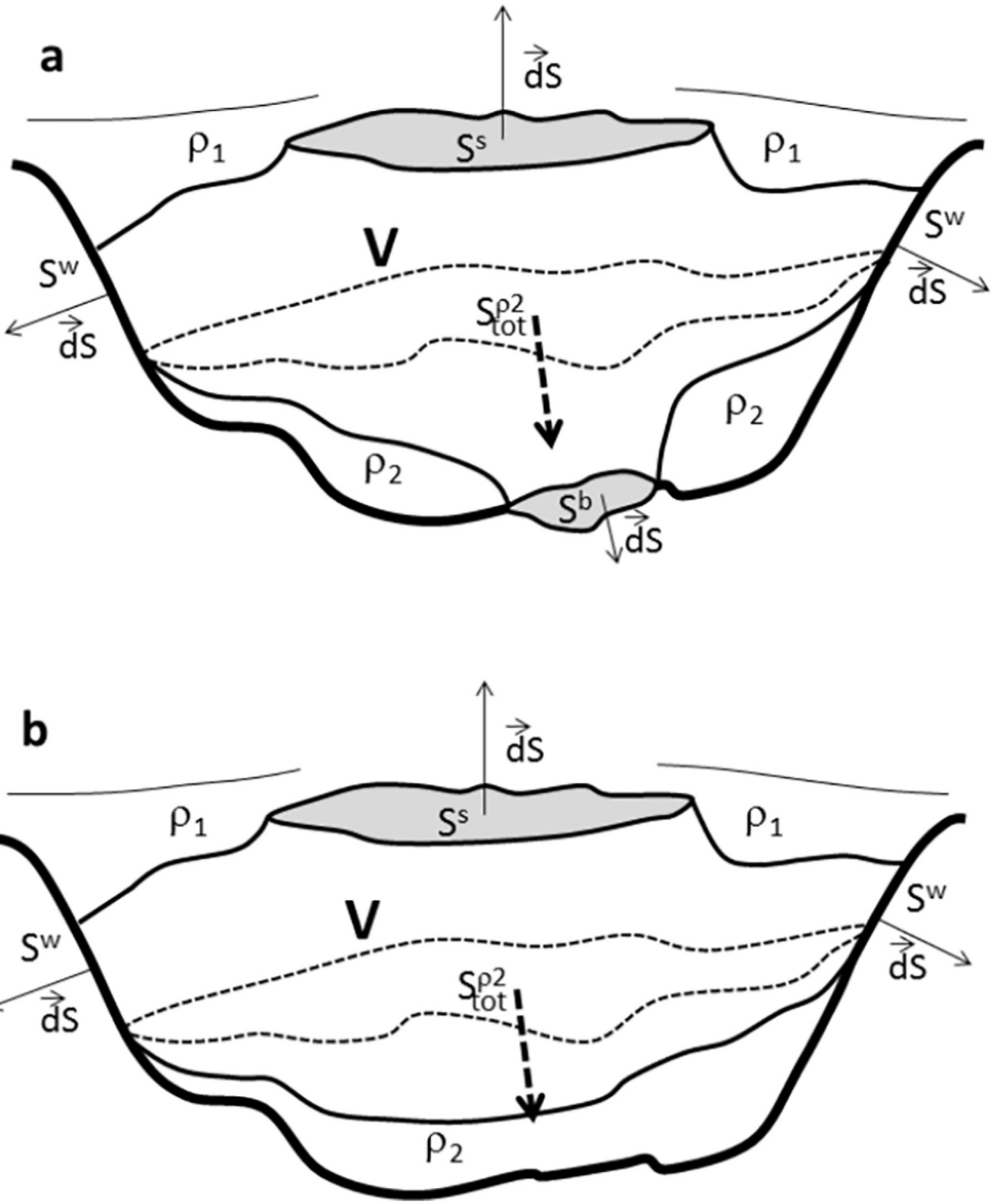
a
dS
ρ1
S^s
ρ1
V
S^w
dS
S^w
dS
S^ρ2_tot
ρ2
ρ2
S^b
dS
b
dS
ρ1
S^s
ρ1
V
S^w
dS
S^w
dS
S^ρ2_tot
ρ2

Figure 4

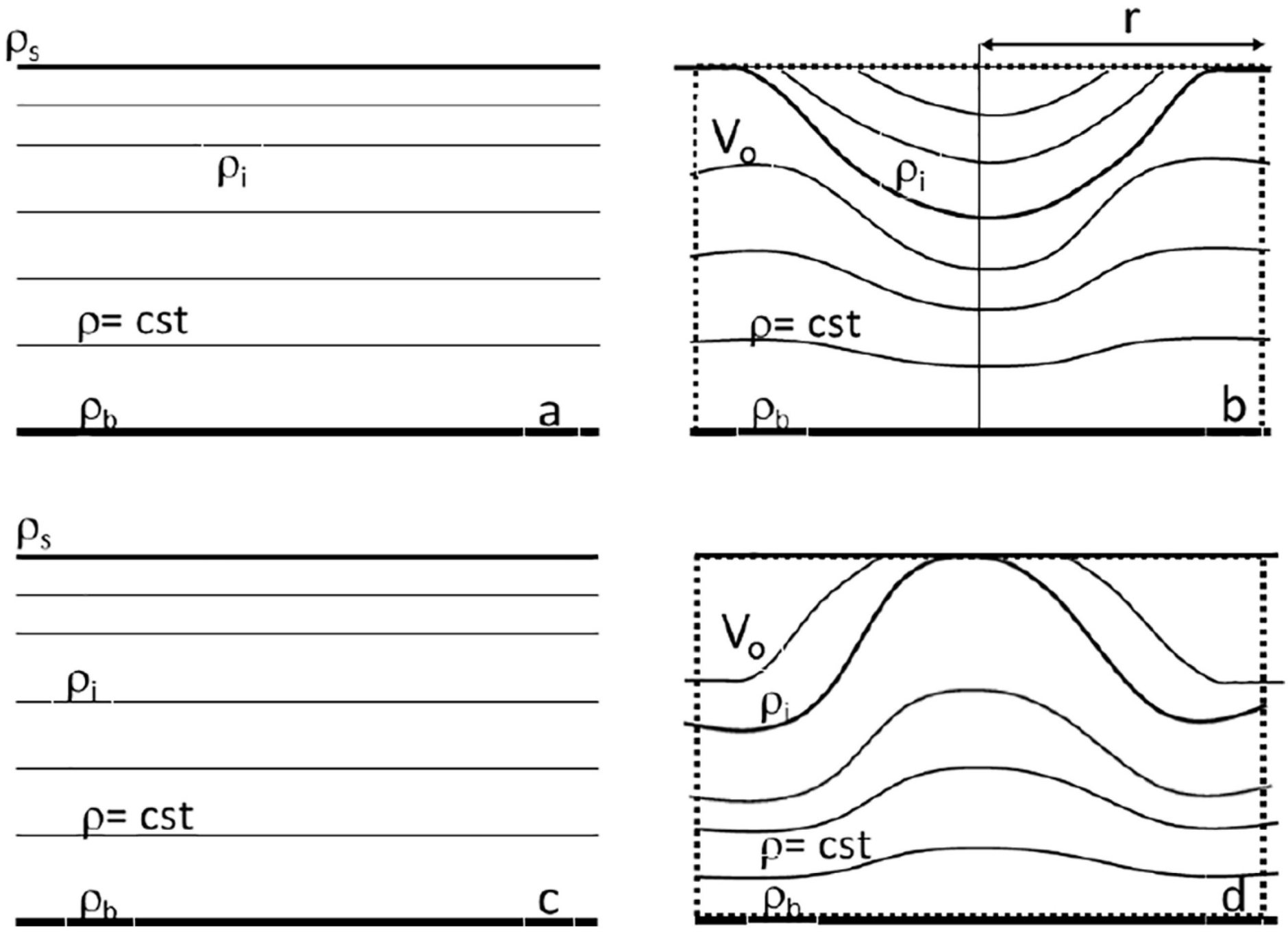

Figure 5

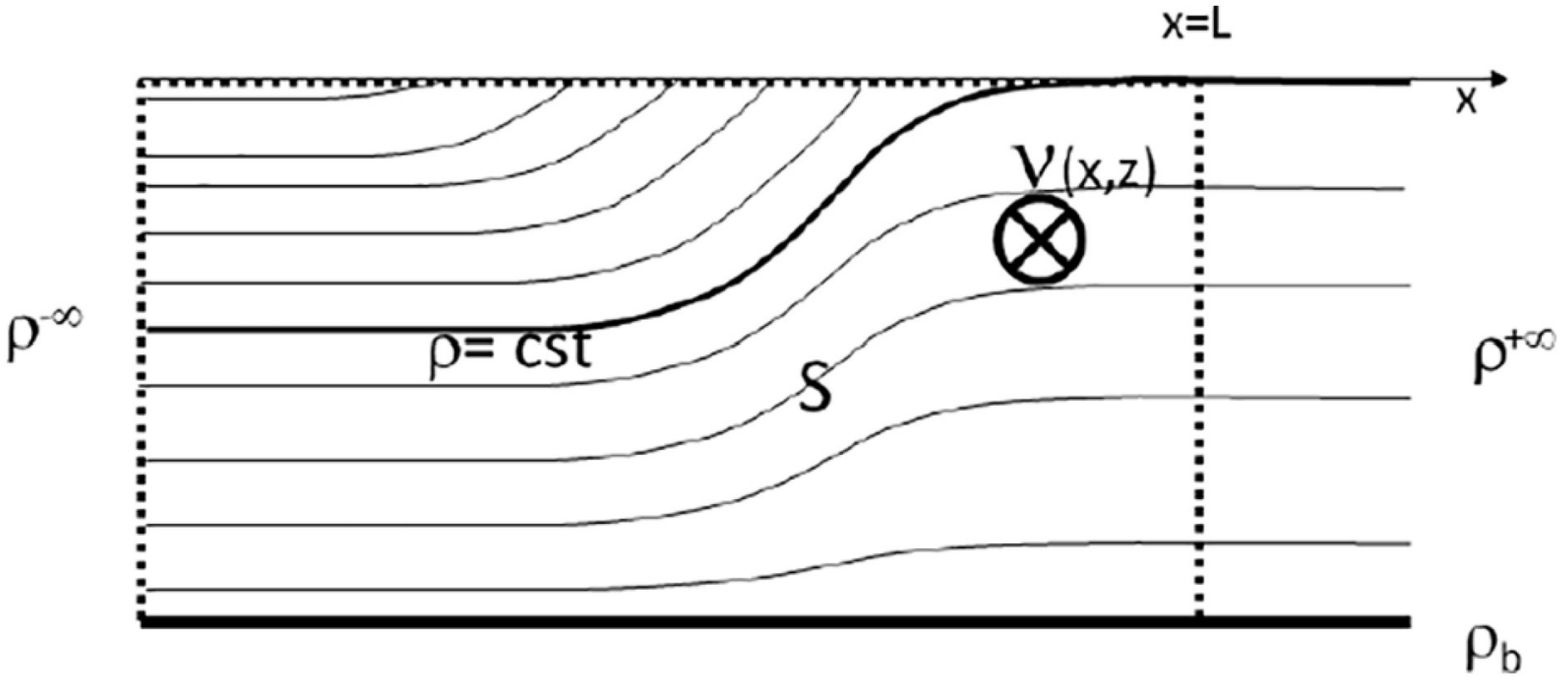

Figure 6

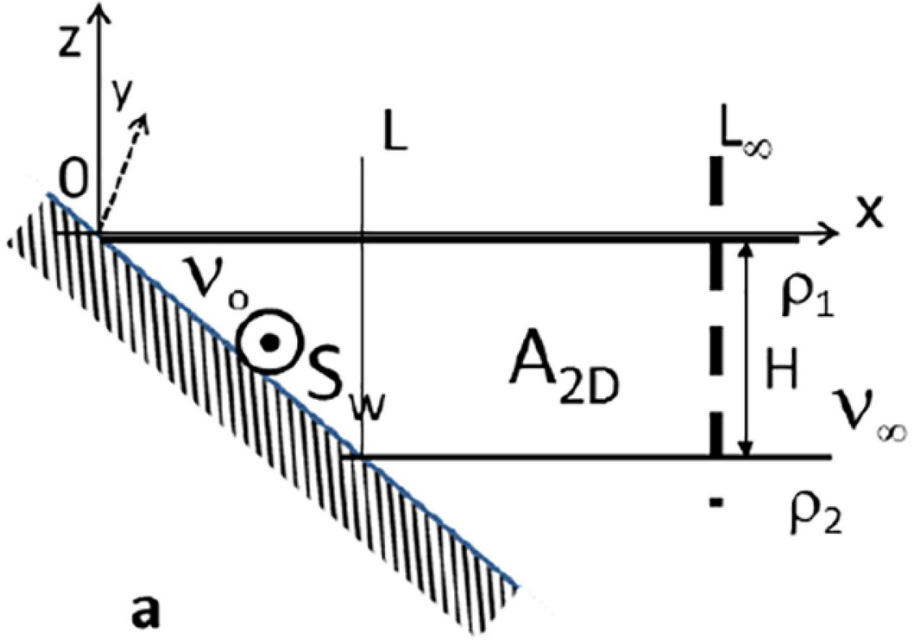

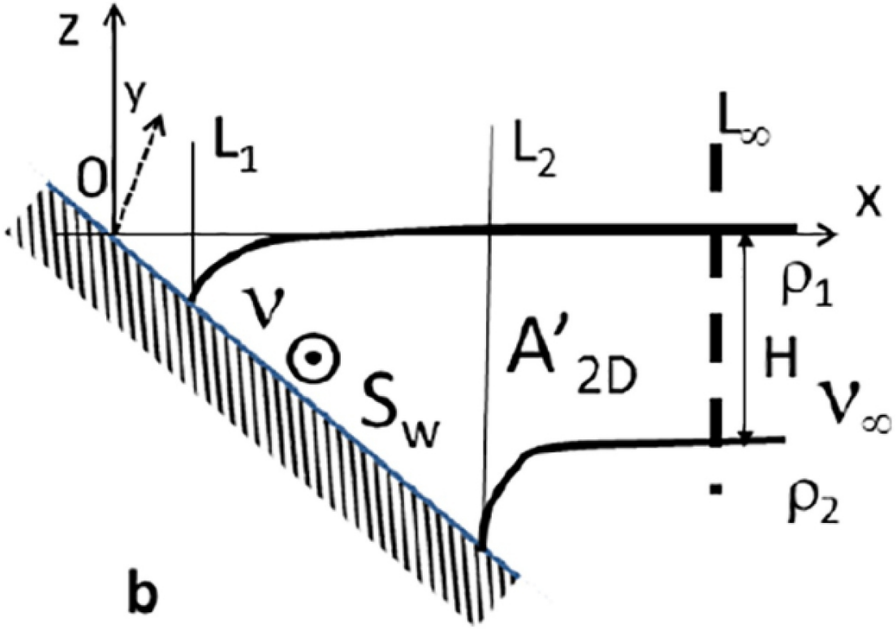

Figure 7

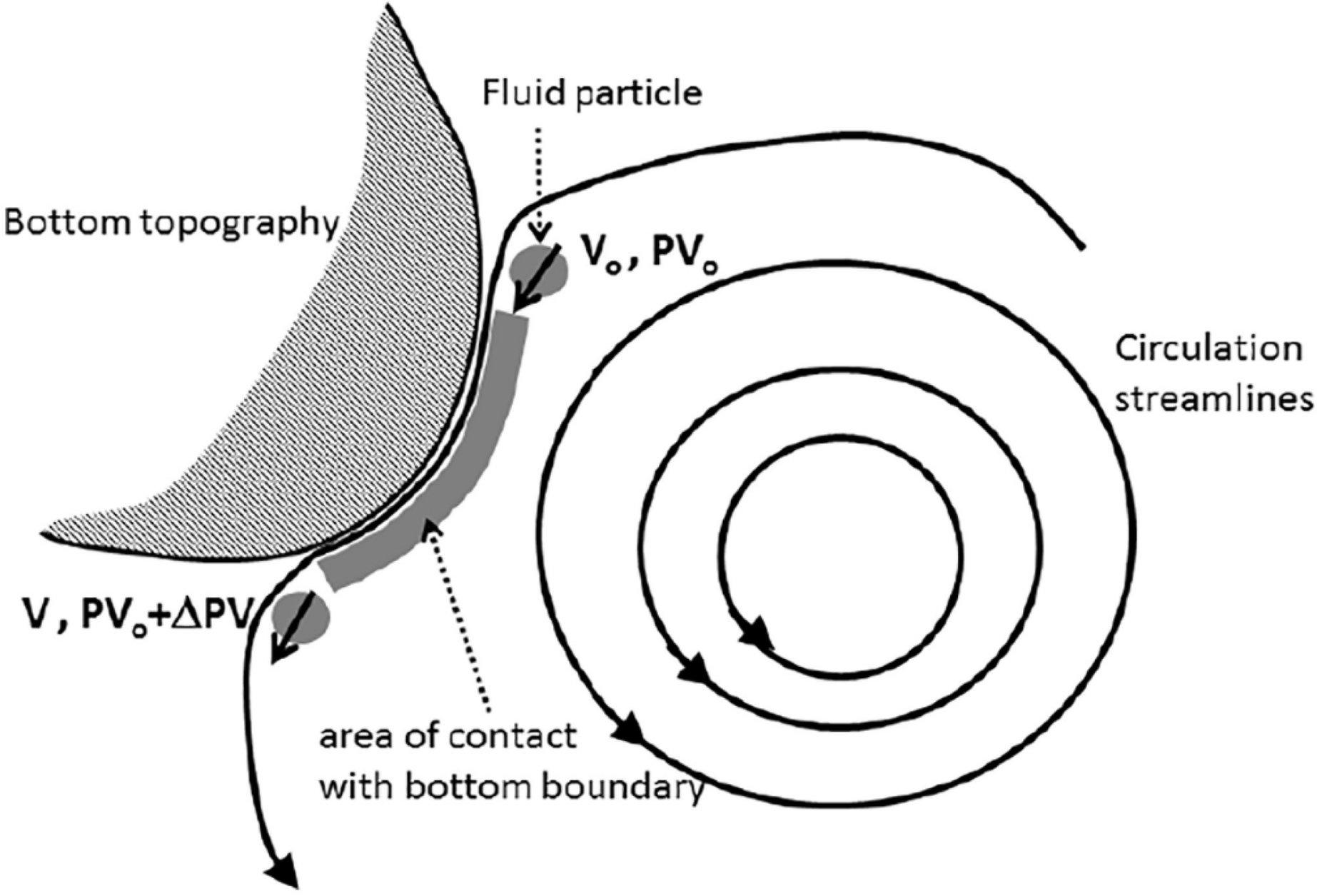
Fluid particle
Bottom topography
V_o, PV_o
Circulation
streamlines
V , $PV_o+\Delta PV$
area of contact
with bottom boundary

Figure 8